Chemical Engineering Science 65 (2010) 3876–3892

Contents lists available at ScienceDirect

Chemical Engineering Science

journal homepage: www.elsevier.com/locate/ces

Analyses of liquid film models applied to horizontal and near horizontal gas–liquid slug flows

R.A. Mazza [a,*], E.S. Rosa [a], C.J. Yoshizawa [b]

[a] Mechanical Engineering Faculty, State University of Campinas, São Paulo, Brazil
[b] PPGERHA, Federal University of Paraná, Paraná, Brazil

ARTICLE INFO

Article history:
Received 28 October 2009
Received in revised form
2 March 2010
Accepted 22 March 2010
Available online 25 March 2010

Keywords:
Multiphase flow
Slug flow modeling
Bubble shape
Fluid mechanics
Mathematical modeling
Numerical analysis

ABSTRACT

An analysis of liquid film models for horizontal and near horizontal gas–liquid slug flows is developed. The models' formulations employ the one dimensional separated phase momentum equations. The formulations differ among themselves, by neglecting some terms on the momentum balance and also on the closure relations. A comparative analysis discloses the differences amongst the formulations. The sensitivity of the liquid film models to the changes on the bubble velocity, liquid slug holdup and liquid viscosity is accessed through a series of parametric runs. Finally, the model is tested against experimental data taken for continuous horizontal slug flow. The tests were designed to check if the models are able to capture the stochastic film properties provided the properly closure relations.

1. Introduction

The slug flow pattern can be viewed by the succession of aerated liquid pistons followed by elongated gas bubbles which are not periodic in time neither in space. The unsteady and non-deterministic nature of the slug flow turns this pattern complex to flow modeling.

The first attempts to model the slug flow neglect its non-deterministic nature by considering the alternating liquid pistons and gas bubbles in an orderly periodic way. The flow is reduced to periodic cells that propagate downstream composed by a liquid piston trailed by gas bubble also named as unit cell (Wallis, 1969). Employing a frame of reference that moves with the bubble nose velocity the picture of a slug unit is frozen in space and the flow is no longer periodic but it is seen as a steady state phenomenon. The unit cell concept bred a number of models for calculating the slug hydrodynamic parameters. The first comprehensive model was developed by Dukler and Hubbard (1975). Further papers employing the unit cell concept improved the steady state slug flow models: Nicholson et al. (1978), Kokal and Stanislav (1989) and Taitel and Barnea (1990).

This paper analyzes the liquid film models first developed as sub-models of the aforementioned unit-cell based mechanistic models. The usefulness of the liquid film models lies on the liquid film holdup estimate. Once the liquid film or the bubble profile is known, it is possible to determine the film length and its averaged holdup through a mass balance. The relevance of the liquid film models goes beyond its application on the unit-cell based models. They are required in slug tracking models to estimate the liquid holdup at the bubble region (see Al-Safran et al., 2004; Cook and Behnia, 2001), and also for the slug initiation at the pipe inlet where the bubbles and slugs are inserted (Nydal and Banerjee, 1994; Barnea and Taitel, 1993; Straume et al., 1992; Grenier, 1997). The liquid film models are also demanded by mixture models such as TACITE described in Pauchon et al. (1994) and also Drift Flux Models (Ishii and Hibiki, 2006). In the former, the liquid film model is useful to estimate the intermittency factor, i.e., the fraction of the liquid film length corresponding to a slug unit. In the last, the liquid film model is used to improve the pressure drop predictions in horizontal and near horizontal slug flows dominated by friction forces. In this case, the knowledge of the liquid film and the slug lengths properly define the wetted surfaces where the shear stresses act. Finally, liquid film models are also demanded by the one-dimensional two-fluid model for slug flow as a sub-model to provide the necessary closure relations, see De Henau and Raithby (1995a,b).

For horizontal and near horizontal pipes the liquid film region has an interface separating the elongated gas bubble at the upper section of the pipe from the liquid film at the lower section. The flow does not possess axis-symmetry, but just a plane of symmetry crossing the pipe's diameter line with a normal orthogonal to the gravity acceleration. The elongated bubble is characterized by three regions: the front, the body and the tail. The first and the last regions range in length between 1 and 3 pipe

* Corresponding author.
E-mail address: mazza@fem.unicamp.br (R.A. Mazza).

0009-2509/$ - see front matter © 2010 Elsevier Ltd. All rights reserved.
doi:10.1016/j.ces.2010.03.035

diameters approximately and are characterized by complex three dimensional flows due to the normal stresses responsible for shaping the bubble's nose and also to the shedding process occurring at the bubble's tail. However, the body of the bubble, much greater than former regions, is reasonably represented as a gas–liquid stratified flow with plane interface at the pipe's cross section.

The shape of the bubble at the nose region exhibits large curvature and the liquid film height with large variations. Benjamin (1968) employing the inviscid theory arrived at the drift velocity of an isolated bubble flowing in a horizontal pipe and its profile. Alves et al. (1993) also employing the inviscid theory extended Benjamin's works to inclined and vertical pipes, taking into consideration surface tension forces. Also Fagundes Netto et al. (1999) employs Benjamin's model to get bubble's nose shape to further develop a liquid film model including the bubble's nose, body and tail region. The shape of the bubble's tail was experimentally studied in the work of Ruder and Hanratty (1990) for horizontal flows. Fagundes Netto et al. (1999) developed an analytical model to the bubble's tail based on the existing similarities between the flow in this region and the hydraulic jump.

Due to the growing interest on slug flow in micro-channels applied to compact heat exchanger and cooling devices, it is necessary to remark that the above description of the bubble's shape applies only to gas–liquid slug flow where the influence of capillary force is negligible. The slug flows in micro-channels are controlled by the viscous and the surface tension forces as described by Bretherton (1961). Some of the bubble's shape features and a liquid film model for slug flow governed by capillary forces are in Abiev (2008) for further reference.

Exploring the fact that the bubble's body is characterized by a region where the liquid film height changes slowly Dukler and Hubbard (1975) were the first to propose an uncoupled free surface film model based on a one-dimensional and steady state channel flow. They arrived at an ODE for the liquid holdup using the liquid momentum equation for a frame of reference that moves at the bubble's nose velocity. Giving the proper initial conditions, the liquid holdup is determined at each pipe cross section using a marching integrating procedure. Nicholson et al. (1978) also used the liquid film model proposed by Dukler and Hubbard, but broaden the model's applicability by properly specifying the initial conditions and acknowledged the bubble's nose velocity dependency on the mixture velocity. Kokal and Stanislav (1989) introduced the interfacial shear stress to the liquid film momentum equation, but neglected any contribution of the gas phase in a version of the separated phase's model at the equilibrium condition. The model advances in respect to the Dukler and Hubbard's model since it considers into momentum balance the shear stresses components at the interface. Taitel and Barnea (1990) use the full, one-dimensional, steady state, separated phases model to capture the gas–liquid interface in horizontal and inclined slug flow with aerated and non-aerated liquid pistons. Distinctly of its predecessor's models, it estimates the liquid film height instead of the pipe's cross section liquid holdup. Andreussi et al. (1993) advanced with the liquid film models considering the liquid film aeration. The authors still use a form of the separated phase momentum equation. The gas phase is modeled similarly to the previous models, but the liquid phase is now considered to be a mixture of dispersed gas bubbles in a continuous liquid film. To date it is the only model which considers the void distribution on the liquid film. More recently, Cook and Behnia (1997) used a force balance to the liquid film and gas bubble which, neglecting the gas density contribution to the gravity force terms, arrive to the simplified form of the liquid film model in terms of either the liquid holdup or the film thickness. Fagundes Netto et al. (1999) also employ the full terms, one-dimensional, steady state, separated phases model to capture the liquid film profile at the bubble region. The model's distinction lies on the solution not in the formulation. Through geometrical and shear stresses approximations they developed an analytical solution to the pipe's cross section liquid holdup.

The liquid film models arise from a set of distinct momentum equations which makes difficult a straightforward comparison. Some models have as dependent variable liquid holdup while others employ the liquid film height. Also, the required closure relations differ among themselves, i.e., the bubble's nose velocity, the liquid slug holdup, the friction factors, etc. Furthermore, some models claim all the shear stresses, inertia terms and gravitational terms while others demand just some of them. The non-similarities among the liquid film models make difficult a beforehand comparison. The objective of this work is to develop a comparison among the models, discuss the relevant terms embodied on the distinct models and also access the models' performance against experimental data taken for liquid film profiles in horizontal slug flow.

The paper is organized as follows: Section 2 presents a unified approach to deduce liquid film models starting from the separated phases' momentum equations (Oliemans and Pots, 2006). The numerical integration procedure is detailed in Section 3. Section 4 describes the experimental facility and the experimental technique used to capture the liquid film height of individual bubbles for an air–water mixture flowing continuously in the slug flow regime. The results, shown in Section 5, start by drawing comparisons among the liquid film models and analyzing the models' sensitivity to some flow parameters such as bubble nose velocity, liquid slug hold up and friction factors among others. Section 5 closes showing some models' features against experimental data taken for horizontal flow. The conclusions are given in Section 6.

2. Liquid film models

An elongated bubble flowing over a liquid film is represented schematically in Fig. 1. The figure has the purpose to introduce the variables that will come to play on the liquid film models. The flow is inside an inclined pipe of angle θ with the horizontal having an internal diameter D. The subscripts G, f and i are used to identify the gas phase, the liquid film and the interface, respectively. U_t is the translational velocity of the bubble's nose; u_G and u_f represent the gas velocity and the liquid film velocity as seen from a stationary observer. Also are represented the relative velocities of the gas and the liquid film from a frame of reference moving with the bubble's nose velocity, v_G and v_f. The abscissas' origin is at the bubble nose pointing downward as indicated in Fig. 1 by the x_f coordinate.

The liquid film models derive from the one dimensional separated phase momentum equations. Choosing a frame of reference moving with the translational velocity of the bubble nose, U_t, the bubble becomes frozen in space and it is possible to eliminate the transient terms leaving a steady state problem to be solved.

The volumetric balances applied to the liquid film and to the gas phase are

$$(U_t-u_f)\alpha_f=(U_t-u_{LS})\alpha_s, \tag{1}$$

and

$$(U_t-u_G)\alpha_G=(U_t-u_b)(1-\alpha_S), \tag{2}$$

where u_G, u_{LS} and u_b represent, respectively, the absolute velocities for the gas phase within the gas bubble and the liquid

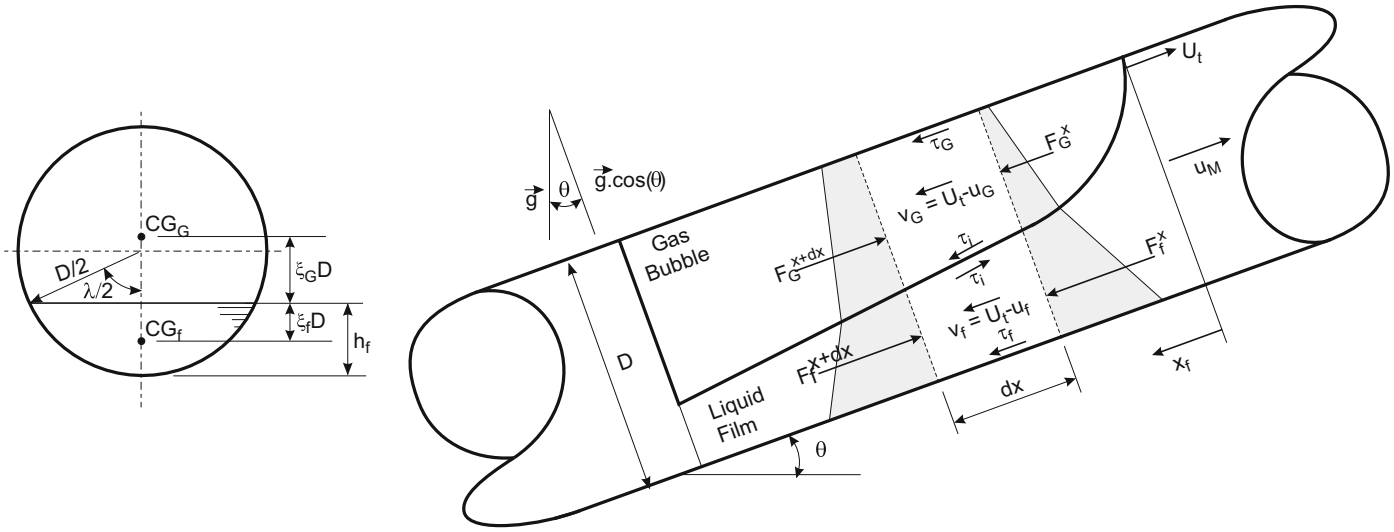

Fig. 1. Schematic diagram for the liquid film region with nomenclature.

and gas phase within the liquid slug, the last as the dispersed bubbles within the liquid slug. Also α_S stands for the liquid slug holdup and α_f and α_G represent the averaged liquid holdup and gas void fraction at the bubble region which are related to each other as

$$A_f = \alpha_f A; \quad A_G = \alpha_G A \quad \text{and} \quad \alpha_f + \alpha_G = 1 \tag{3}$$

The momentum equations for the liquid film and the gas turn to be

$$\frac{d}{dx_f}(\alpha_f \cdot \rho_f \cdot v_f^2) = -\alpha_f \frac{dP}{dx_f} + \frac{S_f}{A}\tau_f - \frac{S_i}{A}\tau_i + \rho_L g \alpha_f \sin\theta - \rho_L g D \frac{d}{dx_f}(\alpha_f \xi_f)\cos\theta, \tag{4}$$

$$\frac{d}{dx_f}(\alpha_G \cdot \rho_G \cdot v_G^2) = -\alpha_G \frac{dP}{dx_f} + \frac{S_G}{A}\tau_G + \frac{S_i}{A}\tau_i + \rho_G g \alpha_G \sin\theta + \rho_G g D \frac{d}{dx_f}(\alpha_G \xi_G)\cos\theta, \tag{5}$$

where P is the pressure; A is the pipe cross section area and ξ_f and ξ_G represent the centroid coordinates of the liquid and gas phases. S_G, S_f and S_i are the wetted perimeters of the gas, liquid film and interface. Finally, the shear stresses at the liquid film, at the interface and at the gas phase are identified by τ_f, τ_i and τ_G. The shear stresses, being frame invariant, are estimated employing the absolute phase velocities together with the corresponding Fanning friction factors:

$$\tau_f = f_f \frac{\rho_f u_f |u_f|}{2}; \quad \tau_G = f_G \frac{\rho_G u_G |u_G|}{2} \quad \text{and} \quad \tau_i = f_i \frac{\rho_G (u_G - u_f)|u_G - u_f|}{2}. \tag{6}$$

The LHS of Eqs. (4) and (5) represent the momentum rate along the pipe axial distance for the liquid and gas phases, respectively. The first term on RHS represents the pressure force term. The phases' shear stresses contributions are in the second and third terms. The gravity force and the hydrostatic force are represented by the fourth and fifth terms.

The use of Eqs. (1), (2), (4) and (5) to model the liquid film profile has some restrictions. The gas and the liquid phases are in complete segregation, i.e., the long gas bubble has no entrained droplets neither the liquid film has dispersed gas bubbles. Complementary, the set of equations does not account for interfacial mass and momentum transfer if one considers the flow of a liquid and its vapor phase. The inertia forces are much greater than the capillary forces, i.e., $We = \rho_L U_M D^2/\sigma \gg 1$, where We is the Weber number. This restriction excludes the existence of slug flow controlled by capillary forces, (Kreutzer et al., 2005). At last, the set of equations is strictly one-dimensional therefore it cannot capture three-dimensional flows' features found at the nose and at the tail of the bubble. At the bubble's nose the liquid film height has a large axial variation, $|dh_f/dx| \gg 1$, which avoids a proper representation by one-dimensional models. At the bubble's tail a distinct process takes place. The liquid phase is accelerated and the gas–liquid interface may evolve in a stair like shape (Fagundes Netto et al., 1999) or even show instabilities in association of gas entrainment. The exact profile at the bubble's tail is governed by complex processes which are poorly captured by one-dimensional models. To comply with the one-dimensional constraint, the set of equations are applied in a region of the liquid film where its height changes slowly, i.e., $|dh_f/dx| \ll 1$ which characterizes Eqs. (4) and (5) as long wave approximations. This region, called bubble's body, lay between the bubble's nose and bubble's tail. , at the bubble's body, the slow changing liquid film height exhibits a low curvature where the surface tension forces are negligible and, therefore, not accounted into momentum balance.

In order to develop the liquid film models is still necessary to make a hypothesis about the shape of the gas–liquid interface to derive the proper geometrical relationship among the film holdup, film height, and wetted perimeters. For horizontal and near horizontal pipes, it is largely accepted that the bubble lies on the upper part of the pipe while the liquid film lies on the bottom. Furthermore, the gas–liquid interface is considered to have a single curvature along the pipe axis while at the pipe cross section it is plane, see schematic representation on the inset of Fig. 1. This condition is typical for flows having low or moderate Froude numbers. To date there is no threshold value for moderate Froude, but it is known that as the Froude or the pipe inclination increases the bubble's nose points toward the center (Bendiksen, 1984) and the gas–liquid interface is no longer plane but starts folding along the pipe radius.

Considering flow regimes and pipe inclinations where the interface is represented by a plane surface at the pipe cross section, the internal angle λ is related to the liquid film height h_f through the trigonometric relation:

$$\lambda = 2\cos^{-1}\left(1 - 2\frac{h_f}{D}\right). \tag{7}$$

Complementary, the liquid film holdup and the wetted perimeters of the gas, liquid film and interface are defined as a function of the

internal angle λ:

$$\alpha_f = \frac{\lambda - \sin(\lambda)}{2\pi}, \tag{8}$$

$$S_G = D\frac{(2\pi-\lambda)}{2}; \quad S_f = D\frac{\lambda}{2} \quad \text{and} \quad S_i = D\sin(\lambda/2). \tag{9}$$

The hydrostatic pressure force terms which appear in Eqs. (4) and (5) also depend on the geometrical properties of the interface. The force is determined by the product between the pressure evaluated at the centroid coordinates, CG, and the pipe's cross section area taken by the phase. The CGs coordinates for the film and for the gas phase are determined as a fraction of the pipe diameter and expressed as a function of the internal angle:

$$\frac{CG_f}{D} = \xi_f = \frac{1}{3\pi\alpha_f}\sin^3\left(\frac{\lambda}{2}\right) - \frac{1}{2}\cos\left(\frac{\lambda}{2}\right), \tag{10}$$

$$\frac{CG_G}{D} = \xi_G = \frac{1}{3\pi\alpha_G}\sin^3\left(\frac{\lambda}{2}\right) + \frac{1}{2}\cos\left(\frac{\lambda}{2}\right). \tag{11}$$

Eqs. (7)–(11) define the relationship among film holdup, film height and interface internal angle as well as the wetted perimeters and the centroid coordinates; variables which are all dependent on the interface geometrical hypothesis.

Considering both phases share the same pressure, one can subtract Eq. (5) from Eq. (4) to eliminate the pressure gradient dependence. Furthermore, substituting the centroid coordinates given by Eq. (10) and (11) one gets

$$\frac{d\alpha_f}{dx_f} = \frac{\frac{S_f}{A}\tau_f - \frac{\alpha_f}{\alpha_G}\frac{S_G}{A}\tau_G - \alpha_f\left(\frac{1}{\alpha_f}+\frac{1}{\alpha_G}\right)\frac{S_i}{A}\tau_i + (\rho_f-\rho_G)\alpha_f g\sin\theta}{\alpha_f\left\{(\rho_f-\rho_G)(g\cos\theta)D\frac{\pi}{4\sin(\lambda/2)} - \left(\frac{\rho_f}{\alpha_f}v_f^2 + \frac{\rho_G}{\alpha_G}v_G^2\right)\right\}}. \tag{12}$$

Using the fact that

$$\frac{dh_f}{d\alpha_f} = D\frac{\pi}{4\sin(\lambda/2)}, \tag{13}$$

Eq. (12) is rewritten in terms of the liquid film height as

$$\frac{dh_f}{dx_f} = \frac{\frac{S_f}{A}\tau_f - \frac{\alpha_f}{\alpha_G}\frac{S_G}{A}\tau_G - \alpha_f\left(\frac{1}{\alpha_f}+\frac{1}{\alpha_G}\right)\frac{S_i}{A}\tau_i + (\rho_f-\rho_G)\alpha_f g\sin\theta}{\alpha_f\left\{(\rho_f-\rho_G)(g\cos\theta) - \left(\frac{\rho}{\alpha}v_f^2 + \frac{\rho_G}{\alpha_G}v_G^2\right)\frac{d\alpha_f}{dh_f}\right\}}. \tag{14}$$

The liquid film profile is estimated using either the liquid film holdup, Eq. (12), or the liquid film height, Eq. (14), in conjunction with the phase mass Eqs. (1) and (2), the definition of the stresses Eq. (6) and the geometrical parameters Eqs. (7)–(9). Both equations convey the same information regarding the liquid film behavior since the liquid holdup and the film height are related through Eqs. (7) and (8). These equations constitute the basis for the liquid film models studied in this work.

The validity of Eqs. (12) and (14) is constrained by the validity of the one-dimensional separated phases momentum equations and by the use of a plane interface. Basically, Eqs. (12) and (14) apply to non-aerated liquid film with negligible surface tension forces and without interfacial momentum transfer. Furthermore, the equations are valid for the bubble's body region where the film height is a slow decreasing function, $|dh_f/dx_f| \ll 1$.

This work chooses seven liquid film models to draw a comparative analysis on the liquid film modeling, accordingly to their representativeness and contribution to the development of the models. In a chronological order the works are: Dukler and Hubbard (1975), Nicholson et al. (1978), Kokal and Stanislav (1989), Taitel and Barnea (1990), Andreussi et al. (1993), Cook and Behnia (1997) and Fagundes Netto et al. (1999). In short these models are referred as DH, NAG, KS, TB, ABN, CB and FFP, respectively. To prove that selected liquid film models stem from Eqs. (12) or (14), each model's equation is retraced starting from one of these root equations.

2.1. Dukler and Hubbard liquid film model (DH)

Dukler and Hubbard (1975) propose an uncoupled liquid film model expressed through the liquid film holdup gradient. The model considers the liquid film flow as free surface channel flow neglecting any influence of the gas phase on the mass and momentum balances. Considering this hypothesis Eq. (12) reduces to

$$\frac{d\alpha_f}{dx_f} = \frac{\frac{S_f}{A}\frac{\tau_f}{\rho_f} + \alpha_f g\sin\theta}{Dg\cos\theta\frac{\pi\alpha_f}{4\sin(\lambda/2)} - v_f^2}. \tag{15}$$

To recover from Eq. (15) the original equation of the Dukler and Hubbard's paper is necessary to use their definition of translational velocity of the bubble nose U_t given as

$$U_t = (1+C)u_{LS}, \tag{16}$$

where C is the constant related to the velocity profile at the liquid slug ahead of the bubble and u_{LS} is the liquid phase velocity within the slug. A volumetric balance for the liquid phase in a frame moving with U_t gives a relationship between the properties of the liquid film and the slug ahead of was given in Eq. (1) and repeated here for convenience:

$$(U_t - u_f)\alpha_f = (U_t - u_{LS})\alpha_s. \tag{1}$$

From Eqs. (16) and (1) it is possible to express the liquid film velocity as a function of the liquid phase velocity within the slug:

$$u_f = Bu_{LS} \quad \text{where } B = \left(1 - C\frac{\alpha_S - \alpha_f}{\alpha_f}\right). \tag{17}$$

Substituting into Eq. (15) the definitions of u_f in Eq. (17), the liquid film shear stress given by Eq. (6) and the film wetted perimeter from Eq. (9) one gets, after some algebraic manipulations, the liquid film holdup expression originally proposed by Dukler and Hubbard:

$$\frac{d\alpha_f}{dx_f} = \frac{\left(f_f\frac{\lambda}{\pi}B^2 + \frac{\alpha_f}{Fr}g\sin\theta\right)}{\frac{D\cos\theta}{Fr}\left\{\frac{\left(\frac{\pi}{2}\right)\alpha_f\sin\left(\frac{\lambda}{2}\right) + \sin^2\left(\frac{\lambda}{2}\right)\cos\left(\frac{\lambda}{2}\right)}{1-\cos(\lambda)} - \frac{1}{2}\cos\left(\frac{\lambda}{2}\right)\right\}} - \left(C\frac{\alpha_S}{\alpha_f}\right)^2, \tag{18}$$

where $Fr = u_{LS}^2/gD$. It is worth to mention that the original expression had a typographical error. The terms $\cos\theta$ and $\cos(\lambda/2)$ were missing as pointed by Nicholson et al. (1978).

2.2. Nicholson, Aziz and Gregory liquid film model (NAG)

Nicholson et al. (1978) starts with the same equation employed by Dukler and Hubbard (1975), Eq. (15). The authors recognized that the bubble's velocity proposed by Dukler and Hubbard was missing the drift term which is important to large diameter pipes and also in inclined flows. They expressed the translational velocity of the bubble as a linear combination of the mixture velocity, u_M, and the propagation velocity of the

elongated bubble in stagnant liquid, also known as drift velocity:

$$U_t = C_0 u_M + C_\infty \sqrt{gD}. \tag{19}$$

Here u_M is the mixture velocity defined as

$$u_M = \left(\frac{Q_L}{A} + \frac{Q_G}{A}\right), \tag{20}$$

where Q_L and Q_G are the phases' volumetric flow rates. The authors also employ the mass balance from Eq. (1) to express the following velocity ratios:

$$\frac{u_f}{u_{LS}} = \left(\frac{U_t}{u_{LS}} - C_f\frac{\alpha_S}{\alpha_f}\right) \quad \text{and} \quad \frac{v_f}{u_{LS}} = C_f\frac{\alpha_S}{\alpha_f} \quad \text{where} \quad C_f = U_t/u_{LS} - 1. \tag{21}$$

Substituting into Eq. (15) the liquid film shear stress, Eq. (6); the film wetted perimeter, Eq. (9); the velocities' ratios, Eq. (21) and, finally, considering horizontal flow, i.e., $\theta = 0$, one gets the expression for the liquid film holdup as proposed by Nicholson et al. (1978):

$$\frac{d\alpha_f}{dx} = \frac{1}{D}\frac{f_f\left(\frac{U_t}{u_{LS}} - C_f\frac{\alpha_S}{\alpha_f}\right)^2\frac{\lambda}{\pi}}{\frac{gD}{u_{LS}^2}\left\{\frac{\left(\frac{\pi}{2}\right)\alpha_f\sin\left(\frac{\lambda}{2}\right) + \sin^2\left(\frac{\lambda}{2}\right)\cos\left(\frac{\lambda}{2}\right)}{1-\cos(\lambda)} - \frac{1}{2}\cos\left(\frac{\lambda}{2}\right)\right\}} - \left(C_f\frac{\alpha_S}{\alpha_f}\right)^2. \tag{22}$$

2.3. Kokal and Stanislav liquid film model (KS)

Kokal and Stanislav (1989) coupled the liquid film model to the gas–liquid interface but not to the gas phase. This assumption reduces Eq. (12) to

$$\frac{d\alpha_f}{dx} = \frac{\frac{S_f}{A}\frac{\tau_f}{\rho_f} - \frac{S_i}{A}\frac{\tau_i}{\rho_f} + \alpha_f g\sin\theta}{(g\cos\theta)D\frac{\pi\alpha_f}{4\sin(\lambda/2)} - v_f^2}. \tag{23}$$

The authors employ to the bubble and liquid film translational velocities, U_t and u_f, the same definitions given in Eqs. (19) and (17). The relative velocity of the liquid film, v_f, is determined using Eq. (21). Substituting into Eq. (23) the absolute velocity of the film, Eq. (17); the relative velocity of the film, Eq. (21); the shear stresses, Eq. (6) and the wetted perimeters, Eq. (9); one arrives to the liquid film model as proposed by Kokal and Stanislav (1989):

$$\frac{d\alpha_f}{dx_f} = \frac{f_f\frac{\lambda}{\pi}\frac{B^2}{D} - f_i\frac{\rho_G}{\rho_f}\frac{4\sin(\lambda/2)}{\pi D}\left(\frac{U_t - Bu_{LS}}{u_{LS}}\right)^2 + \alpha_f\frac{g}{u_{LS}^2}\sin\theta}{\frac{gD}{u_{LS}^2}\cos\theta\left\{\frac{(\pi/2)\alpha_f\sin(\lambda/2) + \sin^2(\lambda/2)\cos(\lambda/2)}{1-\cos(\lambda)} - \frac{1}{2}\cos(\lambda/2)\right\}} - \left(C_f\frac{\alpha_S}{\alpha_f}\right)^2. \tag{24}$$

2.4. Taitel and Barnea liquid film model (TB)

Taitel and Barnea (1990) were the first to include the contributions of the gas phase into the liquid film model. Distinctly from the previous work, they propose a liquid film model based on the liquid film height instead of using the liquid film holdup. The starting point is Eq. (14). Considering the bubble region it is possible to determine the relative liquid film velocity through the mass balance of the liquid phase given by Eq. (1) as

$$v_f = (U_t - u_{LS})\frac{\alpha_S}{\alpha_f}. \tag{25}$$

Similarly, it is possible to get the relative gas velocity from the gas phase mass balance, Eq. (2):

$$v_G = (U_t - u_b)\frac{1-\alpha_S}{1-\alpha_f}, \tag{26}$$

where u_b is the dispersed bubble velocity within the liquid slug evaluated by the drift model (Zuber and Findlay, 1965):

$$u_b = C_b u_M + u_d, \tag{27}$$

where C_b is the distribution parameter and u_d is the drift velocity of dispersed bubbles.

Substituting the relative velocities given by Eqs. (25) and (26) and also using Eq. (3) into Eq. (14) one gets the final form of Taitel and Barnea liquid film model:

$$\frac{dh_f}{dx} = \frac{\frac{S_f}{A_f}\frac{\tau_f}{\rho_f} - \frac{S_G}{A_G}\frac{\tau_G}{\rho_f} - \left(\frac{1}{A_f} + \frac{1}{A_G}\right)S_i\frac{\tau_i}{\rho_f} + \left(\frac{\rho_L - \rho_G}{\rho_L}\right)g\sin\theta}{\left(\frac{\rho_f - \rho_G}{\rho_f}\right)(g\cos\theta) - \left(v_f\frac{(U_t - u_S)}{\alpha_f}\frac{\alpha_S}{\alpha_f} + \frac{\rho_G}{\rho_f}v_G\frac{(U_t - u_b)}{1-\alpha_f}\frac{1-\alpha_S}{1-\alpha_f}\right)\frac{d\alpha_f}{dh_f}}. \tag{28}$$

2.5. Andreussi, Bendiksen and Nydal model (ABN)

The liquid film models based on Eqs. (12) or (14) apply to non-aerated liquid film. This assumption holds for flows with high surface tension liquids at low or moderate velocities. On the other hand, flows with low surface tension liquids at high velocities are likely to have dispersed bubbles in the liquid film. Andreussi et al. (1993) considered the mass flux of the gas phase at the bubble region split into two streams: one that crosses the bubble and the other going through the film underneath the bubble. Furthermore, due to the buoyancy the gas bubbles are progressively released from the aerated liquid film. The volumetric balance for the liquid and gas phase are now rewritten as

$$v_f\alpha_f R_f = (U_t - u_{LS})\alpha_S, \tag{29}$$

$$v_G(1-\alpha_f) + v_f\alpha_f(1-R_f) = (U_t - u_b)(1-\alpha_S), \tag{30}$$

where α_f now represents the pipe cross section area fraction taken by the film and R_f means the liquid holdup on the aerated film. The gas mass transfer at the interface requires an additional closure equation to solve for the aerated liquid film holdup, R_f. The authors propose that the disengagement of gas bubbles is described by a turbulence transfer equation expressed as

$$A\frac{d}{dx}[v_f\alpha_f(1-R_f)] = -\Gamma_f \quad \text{where} \quad \Gamma_f = k_d S_i(1-R_f), \tag{31}$$

and k_d is a mass transfer coefficient.

The gas phase within the bubble and the aerated liquid film are treated as separate phases. The bubbly liquid phase within the film is treated as a homogeneous mixture without slip. Under this assumption the film momentum equation, Eq. (4), turns to be

$$\frac{d}{dx_f}(\alpha_f\cdot\rho_M\cdot v_f^2) = -\alpha_f\frac{dP}{dx_f} + \frac{S_f}{A}\tau_f - \frac{S_i}{A}\tau_i + \rho_M g\alpha_f\sin\theta - \rho_L gD\frac{d}{dx_f}(\alpha_f\xi_f)\cos\theta - \rho_G v_f\Gamma_f, \tag{32}$$

where the last term represents the gas interfacial momentum change and ρ_M is the aerated liquid film density:

$$\rho_M = \rho_f R_f + \rho_G(1-R_f). \tag{33}$$

The gas phase momentum equation differs from Eq. (5) by the interfacial gas transfer and momentum term:

$$\frac{d}{dx_f}(\alpha_G\cdot\rho_G\cdot v_G^2) = -\alpha_G\frac{dP}{dx_f} + \frac{S_G}{A}\tau_G + \frac{S_i}{A}\tau_i + \rho_G g\alpha_G\sin\theta + \rho_G gD\frac{d}{dx_f}(\alpha_G\xi_G)\cos\theta + \rho_G v_f\Gamma_f. \tag{34}$$

Andreussi et al. (1993) neglect the contribution of interfacial momentum term to the film momentum balance. Also, the inertia term of the bubbly liquid film momentum neglects the gas

density, therefore Eq. (32) reduces to

$$\rho_L \frac{d}{dx_f}(\alpha_f \cdot R_f \cdot v_f^2) = -\alpha_f \frac{dP}{dx_f} + \frac{S_f}{A}\tau_f - \frac{S_i}{A}\tau_i + \rho_M g \alpha_f \sin\theta - \rho_L g D \frac{d}{dx_f}(\alpha_f \xi_f)\cos\theta, \quad (35)$$

The inertia and the hydrostatic terms are dropped from the gas momentum equation, Eq. (34) becomes:

$$0 = -\alpha_G \frac{dP}{dx_f} + \frac{S_G}{A}\tau_G + \frac{S_i}{A}\tau_i + \rho_G g \alpha_G \sin\theta. \quad (36)$$

Eqs. (34) and (36) together with the volumetric balances, Eqs. (29), (30) and (31), compound the ABN model. For comparison purposes the momentum equations are re-written in the form of Eq. (14) to get

$$\frac{dh_f}{dx_f} = \frac{\frac{S_f}{A}\tau_f - \frac{\alpha_f}{\alpha_G}\frac{S_G}{A}\tau_G - \alpha_f\left(\frac{1}{\alpha_f}+\frac{1}{\alpha_G}\right)\frac{S_i}{A}\tau_i + \rho_M \alpha_f g \sin\theta}{\alpha_f\left\{\rho_f(g \times \cos\theta) - \left(\frac{\rho_f}{\alpha_f}v_f^2\right)\frac{d\alpha_f}{dh_f}\right\}}. \quad (37)$$

When the film holdup is unity the film's mixture density is equal to the liquid density and Eq. (37) reduces to a complete segregated phases' liquid film model given by

$$\frac{dh_f}{dx_f} = \frac{\frac{S_f}{A}\tau_f - \frac{\alpha_f}{\alpha_G}\frac{S_G}{A}\tau_G - \alpha_f\left(\frac{1}{\alpha_f}+\frac{1}{\alpha_G}\right)\frac{S_i}{A}\tau_i + \rho_f \alpha_f g \sin\theta}{\alpha_f\left\{\rho_f(g \cdot \cos\theta) - \left(\frac{\rho_f}{\alpha_f}v_f^2\right)\frac{\alpha_f}{h_f}\right\}}, \quad (38)$$

which, by its turn, is similar to Eq. (14) if the terms associated with the gas phase density are dropped; namely the weight, the hydrostatic and the inertia terms.

2.6. Cook and Behnia liquid film model (CB)

Cook and Behnia (1997) proposed a model which is almost coincident with Taitel and Barnea (1990) model, the exception is the neglect of the gravity forces applied to the gas component. Consider Eq. (14) as the starting point, dividing both sides by α_f and not considering the gas weight one gets

$$\frac{dh_f}{dx_f} = \frac{\frac{S_f}{A\alpha_f}\tau_f - \frac{S_G}{A\alpha_G}\tau_G - \left(\frac{1}{\alpha_f}+\frac{1}{\alpha_G}\right)\frac{S_i}{A}\tau_i + \rho_L g \sin\theta}{\rho_f g \cos\theta - \left(\frac{\rho_f}{\alpha_f}v_f^2 + \frac{\rho_G}{\alpha_G}v_G^2\right)\frac{d\alpha_f}{dh_f}}. \quad (39)$$

From Eqs. (13) and (9) it is possible to write

$$d\alpha_f/dh_f \equiv S_i/A. \quad (40)$$

Inserting into Eq. (39) the area definitions given in Eqs. (3) and (40) one gets the final form to the liquid film height equation proposed by Cook and Behnia (1997):

$$\frac{dh_f}{dx_f} = \frac{\frac{\tau_f S_f}{A_f} - \frac{\tau_G S_G}{A_G} - \tau_i S_i\left(\frac{1}{A_f}+\frac{1}{A_G}\right) + \rho_L g \sin\theta}{\rho_f g \cos\theta - S_i\left(\frac{\rho_f}{A_f}v_f^2 + \frac{\rho_G}{A_G}v_G^2\right)}. \quad (41)$$

2.7. Fagundes Netto, Fabre and Peresson liquid film model (FFP)

Fagundes Netto et al. (1999) consider the shear stresses components from the film, interface and gas phase but neglect the gas inertia contribution. These assumptions reduce Eq. (12), for horizontal flows, to

$$\frac{d\alpha_f}{dx_f} = \frac{\frac{S_f}{A}\tau_f - \frac{\alpha_f}{\alpha_G}\frac{S_G}{A}\tau_G - \alpha_f\left(\frac{1}{\alpha_f}+\frac{1}{\alpha_G}\right)\frac{S_i}{A}\tau_i}{\alpha_f(\rho_f-\rho_G)(g\cos\theta)\left(D\pi/4\sin(\lambda/2)\right) - \rho_f v_f^2}. \quad (42)$$

The authors consider the sum of the gas and the interfacial shear stress terms approximately equal to the liquid film shear stress at the equilibrium condition. Under this premise Eq. (42) is further simplified to

$$\frac{d\alpha_f}{dx_f} = \frac{\frac{1}{A}\left(\frac{S_f}{\alpha_f}\frac{\tau_f}{\rho_f} - \frac{S_f^\infty}{\alpha_f^\infty}\frac{\tau_f^\infty}{\rho_f}\right)}{\left(\frac{\rho_f-\rho_G}{\rho_f}\right)gD\frac{\pi\alpha_f}{4\sin(\lambda/2)} - v_f^2}. \quad (43)$$

The superscript ∞ represents the equilibrium state, i.e., $d\alpha_f/dx_f = 0$. The liquid film shear stress at equilibrium is evaluated as

$$\tau_f^\infty = f_f^\infty \rho_f \frac{(u_f^\infty)^2}{2}. \quad (44)$$

2.8. Closure equations

This section does not analyze the closure equations but it brings, in a concise form, the closure equations as employed by each liquid film model for comparison purposes. It starts with the bubble's nose velocity, U_t, cast in the form of Eq. (19) for all models. The distribution and the drift velocity parameters, C_0 and C_∞, are presented in Table 1. In this context, the Dukler and Hubbard coefficients are valid only for non-aerated slugs. The estimated values for C_0 range between 1 and 1.29 according to the models. Taitel and Barnea (1990) distinguished C_0 corresponding to the flow regime, laminar or turbulent, while Andreussi et al. (1993) and Fagundes Netto et al. (1999) use a Froude number as a threshold value, both procedures stem from Bendiksen (1984). The models employ different closure relations to the drift velocity: Dukler and Hubbard (1975) neglected the drift velocity; Nicholson et al. (1978) measured experimentally the drift velocity in horizontal flow for pipes of 2.58 cm and 5.12 cm ID; Kokal and Stanislav (1989) used a drift velocity expression suited for upward vertical flows only; Taitel and Barnea (1990) employ a weighted drift velocity expression applied for horizontal, vertical and inclined flows based on Bendiksen (1984); Cook and Behnia (1997) provide a relationship valid only for horizontal flows and finally, Fagundes Netto et al. (1999) provide, for horizontal flow, a drift velocity relation with a surface tension correction factor based on the works of Benjamin (1968) and Weber (1981). The C_0 and C_∞ expressions presented in

Table 1
Coefficients of the bubble translational velocity as proposed by the film models.

Model	C_0	C_∞
DH	$1+0.021\ln(Re_{LS})+0.022$ $30\,000 \le Re_{LS} \le 400\,000$	–
NGA	1.196	$0.27(m/s)/\sqrt{gD}$
KS	1.2	0.345
TB	1.2 for turbulent flow 2 for laminar flow	$0.35\sin\theta + 0.54\cos\theta$
ABN	1.2	0.0 for $Fr_M > 3.5$
CB	1.2	0.542
FFP	1.2 for $Fr_M > 3.5$ 1.0 for Fr_M<3.5	$\left(0.542 - \frac{1.76}{Eo^{0.56}}\right)$ for $Fr_M < 3.5$

$Re_{LS} = Du_{LS}\frac{\rho_f\alpha_f + \rho_G(1-\alpha_f)}{\mu_f\alpha_f + \mu_G(1-\alpha_f)}$, $Fr_M = \frac{u_M}{\sqrt{g \cdot D}}$, $Eo = \frac{(\rho_L-\rho_G)gD^2}{\sigma}$, and σ is the superficial tension.

Table 1 are the facsimile of the expressions proposed by the authors of the respective models. A visual inspection shows that C_0 and C_∞ are evaluated differently by each one raising doubts about their predictions accuracy. These differences should be understood from a historical point of view. A comprehensive work related to the bubble velocity translation was released in 1984 by Bendiksen. Pioneering works prior of 1984, such as DH and NGA used the information available at their time or even limited to their experimental data. The influence of Bendiksen's work is felt on all works after 1984. The value of C_0 equal to 1.2 for turbulent flow regime becomes largely accepted (KS, TB, ABN, CB, FFP), some models also recognize C_0 of 2 for laminar regime (TB) and also some recognized the C_0 Froude number dependence (FFP). All issues were previously addressed by Bendiksen (1984). The drift coefficient, C_∞ followed the same pattern. The values of 0.34 and 0.54 become accepted as the values that C_∞ assumes for vertical and horizontal slug flow on the inertial regime (TB, CB). Also the Froude number dependence of C_∞ is acknowledged in ABN, CB and FFP. At last, FFP introduces a surface tension term correction into drift coefficient. In an attempt to summarize these expressions and include the effects of surface tension the authors propose a general relationship to C_0 and C_∞ based on Bendiksen work presented in Table 5.

Nicholson et al. (1978) employ for holdup at the liquid slug, α_S a closure relation given by Gregory et al. (1978):

$$\alpha_S = \frac{1}{1+(u_{LS}/8.66)^{1.39}}, \tag{45}$$

where u_{LS} is given in meters per second. Taitel and Barnea (1990) is the only model which acknowledges the mass balance for the gas phase, see Eq. (26). They listed seven works reporting expressions for the holdup at liquid slug, α_S, applied to horizontal, vertical and inclined flows taken during the period of 1970 until 1990. The authors do not suggest a specific closure relation to go along with their model. For reference this work adopted the α_S closure relation proposed by Barnea and Brauner (1985) to the TB model:

$$\alpha_S = 1-0.0058\left\{2[0.4\sigma/(\rho_f-\rho_G)g]^{1/2}[(2f_s/D)u_{LS}^3]^{2/5}(\rho_f/\sigma)^{3/5}-0.725\right\}^2, \tag{46}$$

where f_s and σ are the friction factor at the liquid slug and the gas–liquid surface tension. Unfortunately, the liquid holdup estimates proved to be not accurate due to the complex nature of the gas entrainment process happening at the bubble's tail. In fact, this is an active research area and a few recent works on liquid holdup estimates include Abdul-Majeed (2000), Gomez et al. (2000) and Zhang et al. (2003). To perform the mass balance to gas phase is also necessary to estimate the dispersed bubbles' velocity within the liquid slug, u_b. Taitel and Barnea (1990) model the gas velocity within the liquid slug, u_b, employing Eq. (27) with $C_b=1$ and

$$u_d = 1.54\left(\frac{\sigma g(\rho_f-\rho_G)}{\rho_f^2}\right)^{1/4}\sin\theta. \tag{47}$$

The shear stresses are evaluated by Fanning friction factors defined in Table 2 as function of the phases' Reynolds numbers and of the hydraulic diameters

$$Re_k = \frac{\rho_k D_k u_k}{\mu_k} \quad k = \text{f or G}, \tag{48}$$

$$D_f = \frac{4\alpha_f A}{S_f}; \quad D_G = \frac{4(1-\alpha_f)A}{(S_f+S_i)} \tag{49}$$

As observed, all expressions are based on single phase relationships and are explicit for the phases' friction factors. Nicholson et al. (1978) and Taitel and Barnea (1990) friction factor expressions distinguish between laminar and turbulent regimes while the expressions to the others' models apply just for turbulent regime. The pipe's roughness effect on the friction factor is just considered by Kokal and Stanislav (1989) and Taitel and Barnea (1990). For convenience, Fig. 2 brings a comparison

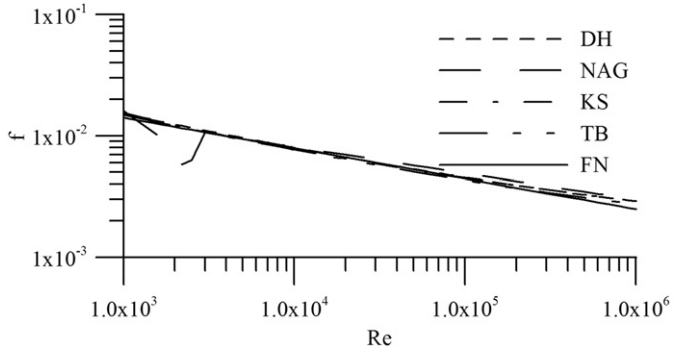

Fig. 2. Friction factors against Reynolds for the various correlations.

Table 2
Fanning friction factors as employed by the models.

Model	Friction factor for the film (k=f) and for the gas (k=G)	Interface, f_i
DK	$f_f = 0.0014+0.125(Re_f)^{-0.32}$	–
NAG	$Re_f \le 2000 \Rightarrow f_f = 16/Re_f$ $2000 < Re_f < 3000 \Rightarrow f_f = 4.51\times10^{-5}\,Re_f^{0.631}$ $Re_f \ge 3000 \Rightarrow f_f = 0.059\,Re_f^{-0.216}$	–
KS	$f_f = \frac{1}{4}\left\{-2\log\left[\frac{\varepsilon}{3.7065D_f}-\frac{5.0452}{Re_f}\log\left(\frac{1}{1.28257}\left(\frac{\varepsilon}{D_f}\right)^{1.1098}+\frac{5.8506}{(Re_f)^{0.8981}}\right)\right]\right\}^2$	$f_i = 1.3\,Re_G^{-0.57}$
TB	$f_k = 0.001375\left[1+\left(2.10^4\frac{\varepsilon}{D_k}+\frac{10^6}{Re_k}\right)^{1/3}\right]$ for rough pipes	horizontal : $f_i = 0.014$ vertical : $f_i = \frac{5[1+300\delta/D]}{1000}$
	$f_k = K\left(\frac{D_k u_k}{\nu_k}\right)^n$ smooth pipes $\begin{cases} k=16\&n=-1 \text{ laminar} \\ k=0.046\&n=-0.2 \text{ turbulent}\end{cases}$	
ABN	Evaluated as single phase friction factors	$f_i = Bf_G$
CB	$f_k = 0.079(Re_k)^{-0.25}$	$f_i = 0.014$
FFP	$f_k = 0.079(Re_k)^{-0.25}$	$f_i = f_G$

δ is the liquid film thickness for vertical flow, ε is the pipe roughness and B is the proportionality constant to the interfacial friction factor.

amongst the several friction factors for smooth pipes including the laminar, turbulent and transitional zones. As expected, the friction factor estimates are almost coincident for Reynolds spanning from 10^3 to 10^6. An exception occurs for the transitional model proposed by Nicholson et al. (1978) where a dimple occurs on the trend line. Briefing, if the expressions for the phases' frictions factors, f_f or f_G, are used within their application range it is a matter of choice, instead of accuracy, to select a correlation. Obviously many other correlations can be used.

For low liquid and gas velocities the gas–liquid interface is likely to be smooth and the interfacial friction factor for smooth surface can be used. As the phases' velocities increase the gas–liquid interface develops waves whose structure determines the interface friction factor. Due to the complex wavy structure of the interface its friction factor, f_i, is not accurately estimated nor has a sound physical model which bears universality to all flow velocities regimes. Kokal and Stanislav (1989) and Fagundes Netto et al. (1999) have the interfacial friction factor estimate equal to the gas phase friction factor, as proposed by Ellis and Gay (1959). Andreussi et al. (1993) estimate the friction factor employing a proportionality factor to the gas phase friction factor. Taitel and Barnea (1990) use for horizontal and inclined flows the proposition given by Cohen and Hanratty (1968).

2.9. Remarks on vertical and off vertical flows

This section is introduced for completeness of the liquid film models. Despite the concern that this paper is on horizontal and near horizontal liquid film models, it was considered convenient at this stage to give some remarks on modeling matters applied to vertical and near vertical flows. The film equations, Eq. (12) or (14), are coupled with the interface geometrical properties by the wetted perimeter, area ratios and centroid coordinates. Also, the relationship between the liquid film height and the film holdup, Eqs. (7), (8) and (13), are strictly related to the interface shape. Once the interface shape is defined these parameters are determined by the geometrical properties of the interface. Since either one of these equations were defined using the hypothesis of a plane interface, their validity extends as long as the interface's shape remains the same.

The extension of their application to upward vertical pipes ($\theta=90^\circ$) is not obvious. Vertical flow is axis symmetric, the long gas bubble does not have contact with the wall but it is centered with the pipe and the liquid film flows on the annular space between the bubble and the pipe wall. At the pipe cross section the gas–liquid interface is described as a concentric cylindrical surface. The changes of shape of the interface result in differences on the relationship between the film holdup and the film height as well as on the interface perimeter. For comparison purposes Table 3 brings the relationships for film height and holdup for plane and concentric interfaces. A visual inspection on Table 3 discloses the differences among the definitions of the geometrical parameters when the interface is plane or concentric; certainly they might have a great influence on the film equations.

Table 3
Geometrical properties for plane and concentric interfaces.

Plane interface (horizontal and inclined flows)	Concentric interface (vertical flows only)
$\alpha_f=\frac{2\cos^{-1}(1-2\frac{h_f}{D})-\sqrt{1-(1-2\frac{h_f}{D})^2}}{2\pi}$	$\alpha_f=1-(1-2\frac{h_f}{D})^2$
$\frac{d\alpha_f}{dh_f}=\frac{4}{\pi D}\sqrt{1-(1-2\frac{h_f}{D})^2}$	$\frac{d\alpha_f}{dh_f}=\frac{4}{D}(1-2\frac{h_f}{D})$
$S_i=D\sqrt{1-(1-2\frac{h_f}{D})^2}$	$S_i=\pi D(1-\frac{h_f}{D})$

Incidentally, Eq. (12) applied to vertical flow has few changes which are quite intuitive. Due to the concentric interface shape the gas phase friction term does not exist on the numerator and the hydrostatic term on the numerator is null because $\theta=90^\circ$, therefore it simplifies to

$$\frac{d\alpha_f}{dx_f}=-\frac{\frac{S_f}{A}\tau_f-\alpha_f\left(\frac{1}{\alpha_f}+\frac{1}{\alpha_G}\right)\frac{S_i}{A}\tau_i+(\rho_f-\rho_G)\alpha_f g}{\alpha_f\left(\frac{\rho_f}{\alpha_f}v_f^2+\frac{\rho_G}{\alpha_G}v_G^2\right)}. \tag{50}$$

Using the chain rule Eq. (50) is expressed in terms of the liquid film height (or thickness) as

$$\frac{dh_f}{dx_f}=-\frac{\frac{S_f}{A}\tau_f-\alpha_f\left(\frac{1}{\alpha_f}+\frac{1}{\alpha_G}\right)\frac{S_i}{A}\tau_i+(\rho_f-\rho_G)\alpha_f g}{\alpha_f\left(\frac{\rho_L}{\alpha_f}v_f^2+\frac{\rho_G}{\alpha_G}v_G^2\right)\frac{d\alpha_f}{dh_f}}, \tag{51}$$

which is valid only if $d\alpha_f/dh_f$is in accordance with the corresponding expression given in Table 3 for concentric interface.

Eqs. (50) or (51) properly express the film's force balance for vertical pipes see for example Fernandes et al. (1983) and Taitel and Barnea (1990). The problem arises for inclined pipes when the interface is neither characterized by a plane nor by a concentric surface. It is likely to occur as the pipe inclination or the flow velocity or both increase due to the displacement of the bubble's nose toward the pipe center. Further increase in these variables eventually lead to eccentric liquid films surrounding the gas bubble which are neither represented by a plane interface nor by a concentric one. It is not known a threshold value where the hypothesis of a plane interface is no longer valid neither is known how accurate is to apply Eq. (12) or (14) for non-plane interfaces. Furthermore, to get a film profile estimate for inclined flows with eccentric interfaces, one still has to develop the expressions to the centroids' coordinates. For small degrees off vertical the hydrostatic term is probably negligible and Eq. (50) or (51) becomes good approximations.

Summarizing, Eq. (12) or (14) is capable to estimate the liquid film profile for horizontal and inclined pipes as long as the interface shape remains plane. For vertical and near off-vertical pipes the film model is represented by Eq. (50) or (51). Other cases still employ Eq. (12) or (14) as an approximation but it is not known its accuracy.

2.10. Ending notes

The liquid film models listed in this section apply to inclined pipe and non-aerated liquid films. The exceptions are the NAG and FFP models which apply to horizontal pipe only and the ABN model which apply to inclined pipes and aerated liquid films. The differences among the non-aerated liquid film models arise due to two factors: (i) neglect of some terms regarding the phases momentum equations and (ii) closure equations, where there is lack of agreement among the U_t, f_i and α_S as proposed by in the original models', see Section 2.8. With the purpose to draw a comparison among the formulation of the non-aerated liquid films' models the ABN model is included considering its particular case where $R_f=1$, see Eq. (38). The models' formulations are casted in the form of Eq. (12) with coefficients (a) through (f) which may be either 0 or 1, see Table 4, depending on the given liquid film model:

$$\frac{d\alpha_f}{dx_f}=\frac{\frac{S_f}{A}\tau_f-(a)\frac{S_i}{A}\tau_i\left[1+(b)\frac{\alpha_f}{\alpha_G}\right]-(c)\frac{\alpha_f}{\alpha_G}\frac{S_G}{A}\tau_G+\alpha_f\rho_f g\sin\theta\left[1-(d)\frac{\rho_G}{\rho_f}\right]}{\alpha_f\rho_f g\cos\theta\frac{A}{S_i}\left[1-(e)\frac{\rho}{\rho}\right]-\rho v_f^2\left[1+(f)\left(\frac{\alpha_f}{\alpha_G}\frac{\rho_G}{\rho_f}\frac{v_G^2}{v_f^2}\right)\right]}. \tag{52}$$

Table 4
Liquid film models' coefficients for Eq. (52).

Models	Coefficients									
	Inclined flows, $\theta > 0^\circ$					Horizontal flows with non-aerated slugs, $\theta = 0^\circ$				
	(a)	(b)	(c)	(d)	(e)	(f)	(a)	(b)	(c)	(e)
DH	0	0	0	0	0	0	0	0	0	0
NAG[a]	not apply						0	0	0	0
KS	1	0	0	0	0	0	1	0	0	0
TB	1	1	1	1	1	1	1	1	1	1
ABN	1	1	1	0	0	0	1	1	1	0
CB	1	1	1	0	0	1	1	1	1	0
FFP[a]	not apply						1	1	1	1

[a] FFP and NAG apply only to horizontal flows.

Eq. (52) includes all terms of the separated phases' momentum equations which represent the inertia, the weight, the hydrostatic and the friction forces for both phases. For this reason it is considered a reference to the other liquid film models as far as the representativeness of the terms are concerned. Under the formulation context of non-aerated liquid film models the TB model embodies all terms of Eq. (52) and DH model only use the terms concerning the liquid film. The other models neglect, partially or completely, the gas phase's terms and also the interface shear, see Table 4. Due the common origin for all models, the output differences among the models may be negligible or not. It depends if the flow conditions comply or not with the applied approximations. For example, if the flow is horizontal or inclined the liquid film models have distinct form due to the gravity force term. For horizontal flows with non-aerated liquid slugs the gas relative velocity is null, $v_G = 0$, as well as the phases' weight because $\theta = 0$. Under these assumptions the FFP and TB become coincident. The CB and ABN omit the gas density ($d = 0$) while TB keeps it ($d = 1$). Since the phases' gravitational weight may become a dominant term in inclined flows it is expected that CB and ABN models give inaccurate estimates for high pressure flow because the gas density is no longer negligible compared with the liquid density. This subject is analyzed in Section 5.

3. Numerical integration and initial condition

In order to solve either Eq. (12) or (14) it is necessary to provide an initial value for α_{fi} or h_{fi} at the origin, $x = 0$. One natural choice for initial value is to force a match with the liquid holdup of the liquid piston in front of the film (Taitel and Barnea, 1990):

$$\text{at } x = 0, \quad \alpha_{fi} = \alpha_s \quad \text{or} \quad \frac{h_{fi}}{D}, \tag{53}$$

where h_{fi} corresponds to a liquid film height equivalent to α_{fi}. Furthermore, as the bubble lies on the upper part of the tube, it is also expected that α_f or h_f/D always decreases as x distance increases until, eventually, it reaches an equilibrium value, i.e., $d\alpha_f/dx = dh_f/dx = 0$. Unfortunately, there are some flow conditions which, replacing α_{fi} or h_{fi} into Eq. (12) or Eq. (14), results in $d\alpha_f/dx > 0$ or $dh_f/dx > 0$, this is clearly inconsistent with the physical evidences. To fix α_{fi} or h_{fi} for these flow conditions they have to be progressively reduced until $d\alpha_{fi}/dx < 0$ or $dh_{fi}/dx < 0$ are met. This procedure was explicitly stated in the works of Nicholson et al. (1978), Taitel and Barnea (1990), Cook and Behnia (1997) and Fagundes Netto et al. (1999). Taitel and Barnea (1990) bring a physical explanation on the grounds of a phenomenon related to supercritical channel flow. If h_{fi} is greater than a critical value the initial height is instantaneously reduced to the critical value.

Table 5
Default parameters of the bubble translational velocity.

	C_0		C_∞
$Re_M \geq 2000$	$Fr_M \geq 3.5$	1.2	$\frac{0.345}{(1+3805/Eo^{3.06})^{0.58}}\sin\theta$
	$Fr_M < 3.5$	1.0	$\left(0.542-\frac{1.76}{Eo^{0.56}}\right)\cos\theta+\frac{0.345}{(1+3805/Eo^{3.06})^{0.58}}\sin\theta$
$Re_M < 2000$		2.0	$\left(0.542-\frac{1.76}{Eo^{0.56}}\right)\cos\theta+\frac{0.345}{(1+3805/Eo^{3.06})^{0.58}}\sin\theta$

where $Re_M = \frac{\rho_L u_M D}{\mu_L}$, $Fr_M = \frac{u_M}{\sqrt{gD}}$ and $Eo = \frac{(\rho_L-\rho_G)gD^2}{\sigma}$.

At last, the coordinate $x = 0$ is not the coordinate where the bubble nose is but it is where the numerical integration starts. Strictly, $x = 0$ should be the beginning of the bubble's body region, as stated in Section 2. Unfortunately this position is not known in advance, it must be approximately between one to three pipe diameters far from the bubble's nose. In practice the length from the beginning of the bubble's body to the bubble's nose is disregarded and $x = 0$ is considered to represent the position of the bubble's nose. This approximation holds when the film length is much greater than the extent of the bubble's nose region.

All non-aerated liquid film models have similar integration procedures. The dimensionless liquid film height is used to illustrate the integration procedure based on Eq. (14). The next axial distance, x_f^{i+1} is evaluated numerically in terms of constant increments on the liquid film height, Δh_f, and of the reciprocal of Eq. (28) evaluated at step 'i'

$$x_f^{i+1} = x^i + \Delta h_f \left(\frac{dh_f}{dx}\right)^{-1}. \tag{54}$$

The initial condition correspond to $i = 0$; $x_f^0 = 0$ or the distance from the bubble nose if one has it available also $(dh_f^0/dx)^{-1}$ is evaluated at $h_f^0 = h_{fi}$. Eq. (54) depends on the geometrical parameters S_f, S_i and S_G, on the phases' transport properties ρ_k and μ_k (k = f or G), on the shear stresses, and on the phases' weight which are evaluated at each h_f step.

The sensitivity of the step size on the numerical integration is accessed using a test case applied to Eq. (14). It consists of a water–air mixture, at near atmospheric pressure and ambient temperature, flowing horizontally in a 26 mm ID smooth pipe in the slug flow regime. The water and the air superficial velocities are 0.33 m/s and 1.67 m/s. In terms of dimensionless parameters these flow conditions give: Re_M, Fr_M and Eo of 78 000, 4 and 100, respectively, as defined in Table 5. The test employs four h_f/D steps of 10^{-1}, 10^{-2}, 10^{-3} and 10^{-4}. Fig. 3 shows the liquid film profile for the distinct integration steps. It is observed almost no

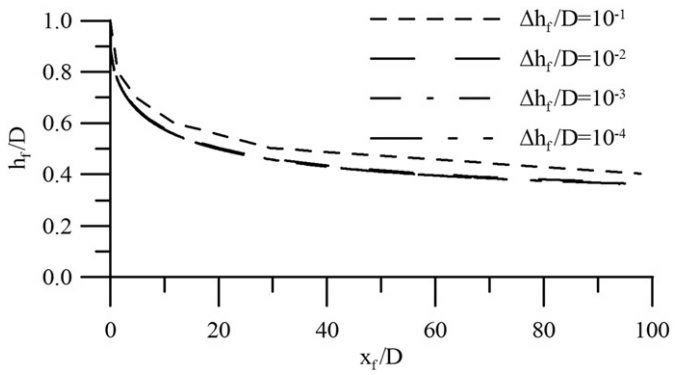

Fig. 3. The influence of the step size on the numerical integration of the film profile.

changes on the liquid film profiles for step sizes smaller than 0.01 pipe diameter. The present analysis employs a step size of 0.0001D for all simulations.

4. Experimental facility

The test section is a 26 mm ID straight, horizontal and transparent Plexiglas pipe 900 pipe diameters long, i.e., 23.4 m. The working fluids were compressed air and ordinary tap water. Three air compressors and a centrifugal pump supply the air and the water to the mixer installed at the entrance of the test section. At the end of the test section the mixture is discharged, without restraint, into a receiving tank open to the atmosphere. The air is treated as an ideal gas. The ordinary tap water has density of 999 kg/m^3 and dynamic viscosity of 0.001 Pa s. The liquid flow-rate was measured by a Micro-Motion® Coriolis mass type flow meter accurate within 1%. A Merian laminar flow element was used to measure the air flow-rate with reported uncertainty of $1\frac{1}{2}$%. The range of water and air superficial velocities span, respectively, between 0.25–1.35 m/s and 0.4–1.7 m/s at ambient pressure and temperature (94.7 kPa @ 21 °C).

The liquid film height, the liquid film length and the bubble velocity were measured by a twin set of double wire conductive probes placed 777D downstream the mixer and spaced 50 mm from each other. Each double wire probe consists of a pair of gold wires with 100 μm stretched along the pipe diameter. The probe picks up the variation of the air and water electrical conductance between the parallel wires (Koskie et al., 1989). The circuit is driven by a 12 kHz oscillator. The output signal is amplified and filtered with a cutoff frequency of 8 kHz to remove the carrier frequency. The media conductivity, so does the probe, is sensitive to changes in the temperature or in the water pH. To exclude these undesirable changes a slave probe is used to measure only the conductance changes due to temperature or water pH changes. The output voltage signal is mapped into the liquid film heights through measurement of static film heights.

The twin voltage signals resemble square waves shifted in time due to the probes' spacing. The high and low values correspond to the occurrence of the water and the air, respectively. The signals were sampled at 3 kHz, digitized and stored by a National Instruments data acquisition system. The sampled signals represent, at the same time, the residence time of the two phases as well as the instantaneous liquid film profile of a given liquid film. The bubble's nose velocity of each elongated bubble is determined by the time interval required for the interface to move from one probe to the other. The liquid film lengths were determined by multiplying the residence time of the gas bubble over the probe by the bubble nose velocity. The stochastic properties of the liquid film height, liquid film length and bubble velocity stem from measurements performed in a bubble population ranging from 300 to 600 units for each experimental run.

5. Analyses

This section has three objectives: compare the liquid film profiles amongst the models; develop a sensitivity analysis of a model to certain flow parameters for horizontal and near off horizontal pipe's inclination and compare the liquid film estimates against experimental data for horizontal pipe.

To develop the sensitivity analysis and the comparisons against experimental data the employed liquid film model and associated closure equations have to be defined recurrently along this section. To avoid unnecessary repetition they are defined here instead. The employed liquid film model consists of the volumetric balances defined in Eqs. (1) and (2) together with the film equation, Eq. (14). The default closure equations, unless stated otherwise, have the following definitions: (a) liquid piston holdup, $\alpha_S=1$; (b) phases friction factor for smooth walls $f_k=0.079\ (\mathrm{Re}_k)^{-0.25}$ if turbulent, otherwise $f_k=16/\mathrm{Re}_k$; (c) interfacial friction factor, $f_i=0.014$ and (d) bubble velocity given as $U_t=C_0u_M+C_\infty\sqrt{gD}$ where C_0 and C_∞ are coefficients that depend on the mixture Reynolds and Froude numbers which follows the Bendiksen (1984) proposition. For horizontal flow it employs a drift coefficient given by Benjamin (1968) with the surface tension correction of Weber (1981). For vertical flow it uses the drift coefficient given by Viana et al. (2003) since $\sqrt{D^3g(\rho_L-\rho_G)\rho_L}/\mu_L>200$. For reference the values of the coefficients are shown in Table 5. For analyzes purposes it is employed a 26 mm ID pipe with inclination spanning from horizontal up to 30° off horizontal. Unless stated otherwise, the working fluids are air and water at ambient pressure and temperature; $\rho_G=1.17\mathrm{kg/m^3}$ and $\rho_L=998\ \mathrm{kg/m^3}$.

The analyses of the results from Eq. (14) are based on three dimensionless groups: Re_M, Fr_M and Eo, see definitions in Table 5, and on three operational parameters: pressure, liquid density and liquid viscosity. The mixed approach based on dimensional and non-dimensional parameters allows a straightforward use of the results but lack of generalization. On the other hand, an analysis based only on dimensionless groups grants generalization of the results but it is cumbersome. It would involve dimensionless parameters such as friction factors, wetted perimeters and void fractions which depend among themselves as well as on the Re_M and Fr_M. The implicit dependency among the parameters overshadows the analyses once it is not possible to change a single parameter keeping the others fixed.

5.1. Comparison amongst the liquid film models

Three tests were chosen to access the similarities and non-similarities amongst the liquid film models. They apply to a water–air mixture flowing horizontally in a 26 mm ID smooth pipe in a turbulent flow regime. Test no. 1 is considered to be a reference with near atmospheric pressure with water and air superficial velocities of 0.33 and 1.67 m/s, respectively which renders a Fr_M of 4. Test no. 2 has the same conditions of Test no. 1 but the pressure is 10^7 Pa, typical of offshore deep water oil producing pipelines. Finally, Test no. 3 has the same conditions of Test no. 1 except that the water and air superficial velocities increased to 1 and 10 m/s, respectively, or Fr_M of 22. A summary of the test parameters is presented in Table 6. The tests, grouped into series A and B, apply to DH, NAG, TB and FFP models. The CB and ABN models, the last restricted to non-aerated film

Table 6
Test parameters for series A and B.

Parameter	Units	Test no. 1	Test no. 2	Test no. 3
J_L	m/s	0.33	0.33	1
J_G	m/s	1.67	1.67	10
ρ_G	kg/m^3	1.17	117	1.17
ρ_f	kg/m^3	998	998	998
μ_G	Pa s	1.7×10^{-5}	1.7×10^{-5}	1.7×10^{-5}
μ_f	Pa s	1.0×10^{-3}	1.0×10^{-3}	1.0×10^{-3}
σ	0.07	0.07	0.07	0.07
Re_M	–	52 000	52 000	285 000
Fr_M	–	4	4	22
Eo	–	95	84	95
Series A closure relations		as given by the specific model		
Series B closure relations		default closure relations defined at the beginning of Section 5		

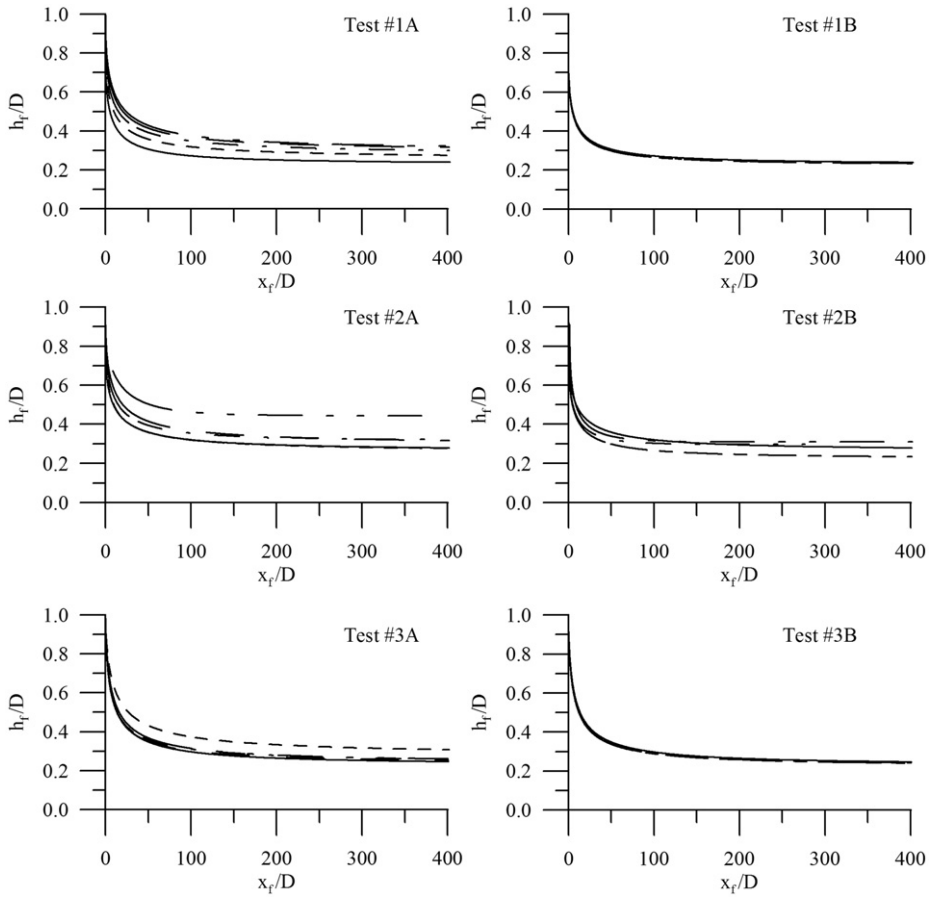

Fig. 4. Liquid film profile for series A and B tests. ——— FFP; - - - - - - - DH; — · — · — · KS; — — — — · NAG; — · · — · · — TB.

conditions, for employing almost the same terms as the TB model were dropped for clarity and conciseness of the figures. The series A tests applies the selected liquid film models with their corresponding closure relations as listed in Tables 1 and 2 with $\alpha_S=1$ for all models. The series B tests mirror series A test parameters, but all selected liquid film models employ the default closure relations as defined at the beginning of this section. The series B tests were designed to disclose differences amongst models due to the approximations embodied on the formulations because it applies the same closure relations in all models.

The series A film profiles are shown in Fig. 4. They exhibit differences from nose to tail along their 400 D of extension. For Test no. 1A, at $x_f/D=400$ the dimensionless liquid film height estimates spans from 0.24 to 0.32. The highest values were given by TB model and the lowest by FFP. The profiles are somewhat similar for TB, KS and NAG models. Increasing the pressure, Test no. 2A, TB model gives the highest estimates. The NAG and KS models have paired results and the FFP and DH models exhibit the lowest estimates. Finally, increasing the mixture velocity, Test no. 3A, there is again a mismatch among the models. The TB, FFP, KS and NAG models have similar results while DH model displays a thicker film estimate. The series A tests show some consistency for the NAG and KS outcomes, they were always similar for the distinct test conditions. Nevertheless, it is not possible to conclude if the differences on the outcomes are due to the closure equations or to the embodied approximations on the formulation. In regard to this matter series B tests were devised having the same closure relations for all tested models.

At atmospheric pressure and Fr_M of 4, Test no. 1B, all models estimate the same liquid film profiles (see Fig. 4). This result discloses two aspects of the models: (i) the differences on the outcomes observed on Test no. 1A are due to the lack of agreement among the closure relations and (ii) at near atmospheric pressure and moderate velocities the approximations embodied on the models' formulation are equally good. In other words, DH model, the simplest model, is as good as the full term formulation of TB model. Under the assumptions of Test no. 1, the liquid shear stress is dominant over the gas and interfacial shear stresses and the gas density has negligible contribution to the hydrostatic term. When the pressure increases, Test no. 2B, some differences amongst the models come out as shown in Fig. 4. The outcomes are paired into two groups: DH and NAG models form one group while the models TB, KS and FFP constitute the other group. These differences arise because the DH and NAG group does not account for the interfacial gas phase shear stresses which, being dependent on the gas density no longer can be neglected, see Eq. (15). Finally, when Fr_M is 22 or the mixture velocity is increased by a factor of $5\frac{1}{2}$, Test no. 3B, any significant differences is not observed amongst the models as shown in Fig. 4. This result shows that the liquid phase inertia is properly accounted for all tested models. Again, the differences among liquid film models outputs displayed on Test no. 3A are due to the mismatch on the employed closure relations.

5.2. Model sensitivity: analysis based on the height of equilibrium

The equilibrium height of film happens when the film height no longer changes, i.e., $dh_f/dx=0$. While the film profile gives the local height, the equilibrium height condenses the profile information to a single value at the equilibrium condition. This form allows analyzing the model's sensitivity to the closure equations over a broad range of parameters including mixture Froude numbers, pipe inclinations and operational pressure. At the equilibrium condition the film equation, Eq. (12) or (14), reduces to a balance between shear stresses and gravity forces:

$$\frac{S_f}{A}\tau_f-\frac{\alpha_f}{\alpha_G}\frac{S_G}{A}\tau_G-\alpha_f\left(\frac{1}{\alpha_f}+\frac{1}{\alpha_G}\right)\frac{S_i}{A}\tau_i+(\rho_f-\rho_G)\alpha_f g\sin\theta=0. \quad (55)$$

Eq. (55) has no general analytical solution for α_f due to the complex algebraic relations between α_f and the wetted perimeters and also to the friction terms. There is though a particular case where an analytical solution is possible if one considers horizontal flow with negligible gas and interfacial friction forces, these approximations are the same used by DH model. The only possible solution to Eq. (55) is $u_f=0$ which, substituting into Eq. (1), one finds the film holdup at equilibrium as

$$\alpha_{f,\infty}=\left(1-\frac{u_{LS}}{U_t}\right)\alpha_S. \quad (56)$$

The liquid phase velocity within the liquid slug, u_{LS}, is estimated considering the volumetric balance on the liquid slug:

$$u_M=u_{LS}(\alpha_S)+u_b(1-\alpha_S). \quad (57)$$

The gas phase velocity, u_b, is estimated with Eq. (27). Substituting Eqs. (27) and (57) into Eq. (56) one gets an approximate expression to the liquid holdup at equilibrium as a function of the mixture velocity (Nicholson et al., 1978):

$$\alpha_{f,\infty}\cong\left(1-\frac{u_M}{U_t}\right)\alpha_S. \quad (58)$$

Eq. (58) discloses that at equilibrium the film holdup increases as α_S and U_t increases which, although useful, has its application limited to horizontal flows ($\theta=0$) and low pressure where the gas and the interface force friction forces are negligible. The sensitivity analysis is extended to other operational conditions only by means of a numerical solution of Eq. (55). This work explores pipe inclinations limited up to 30° off horizontal as an attempt to assure that for all operational conditions the gas–liquid remained plane, otherwise the employed interface geometrical relationships are no longer valid.

Fig. 5 brings the dimensionless equilibrium height as a function of the pipe inclination. In particular, Fig. 5a–c shows the equilibrium height sensitivity to the following operational parameters: the mixture Froude number (a); the operational pressure (b); the liquid phase density (c). Complementary, Fig. 5d–f disclose the model's sensitivity related to the following closure equations: bubble's nose velocity (d); the liquid piston holdup (e) and finally the interfacial friction factor (f). The analysis drawn in Fig. 5, except for (a), employs two mixtures Froude numbers of 2 and 22 which are represented, respectively, by the thin and thick continuous lines. The low and the high values of Fr_M were chosen as representatives of a lower and an upper bound to operational Fr_M in commercial pipelines. The low and high values of Fr_M correspond to mixture Reynolds of 26 000 and 286 000 for an air–water mixture flowing in a 26 mm ID pipe at near atmospheric pressure and ambient temperature.

The equilibrium height for pipe inclination changing from horizontal up to 30° upward is shown in Fig. 5a for mixture Froude numbers changing from zero (only drift) up to 22. Except for $Fr_M=0$, all other Froude values rendered liquid pistons in the turbulent regime. For $Fr_M<2$ the equilibrium height is quite sensitive to the pipe inclination. A fraction of a degree off the horizontal causes large changes on the equilibrium height. This effect is felt up to pipe inclinations less than 10°. For pipe inclinations between 10° and 30° it is observed a slow decreasing behavior of the equilibrium height as the pipe inclination increases. On the other hand, for $Fr_M>10$ is observed a low sensitivity of the equilibrium height with the pipe inclination at angles near off the horizontal. Actually, the equilibrium height exhibits a slow decreasing behavior as the pipe inclination increases from horizontal up to 30°.

The sensitivity of the equilibrium height on operational pressure at distinct pipe inclinations is shown in Fig. 5b. The thin and thick continuous lines represent Fr_M of 2 and 22 at atmospheric pressure, $P_{atm}=10^5$ Pa. Complementary, the thin and thick dashed lines correspond to Fr_M of 2 and 22, respectively, but evaluated at 10^7 Pa, typical of offshore deep water oil producing pipelines. At high pressure the equilibrium height is raised as compared at atmospheric pressure for the same Fr_M. Considering Fr_M of 2 the differences on the equilibrium height attain 45% at horizontal and near off horizontal and decrease to 15% as the pipe inclination increases up to 30°. The differences on the equilibrium height for Fr_M of 22 are almost uniform and equal to 47% through all pipe inclination range. Liquid film models do not acknowledge the interface and gas phase terms do not capture this effect, as seen already seen in Section 5.1

The change on the liquid density does not affect the equilibrium height at low pressure because the liquid density is, typically, three orders of magnitude greater than the gas density. But, operation at high pressure discloses the model's sensitivity to the liquid phase density, see Fig. 5c. The thin and the thick continuous lines represent, respectively, Fr_M of 2 and 22 at 10^7 Pa of an air and water mixture. Additionally, the thin and thick dashed lines have the same operational conditions but the liquid phase density is of 800 kg/m^3, representative of crude oils. The decrease on the liquid phase density causes a mild increase in the height of equilibrium. At Fr_M of 2, through all pipe inclinations, the changes on the height of equilibrium are quite small. The effect of the density change is felt at Fr_M of 22 where an increase of nearly 6% is observed in the equilibrium height.

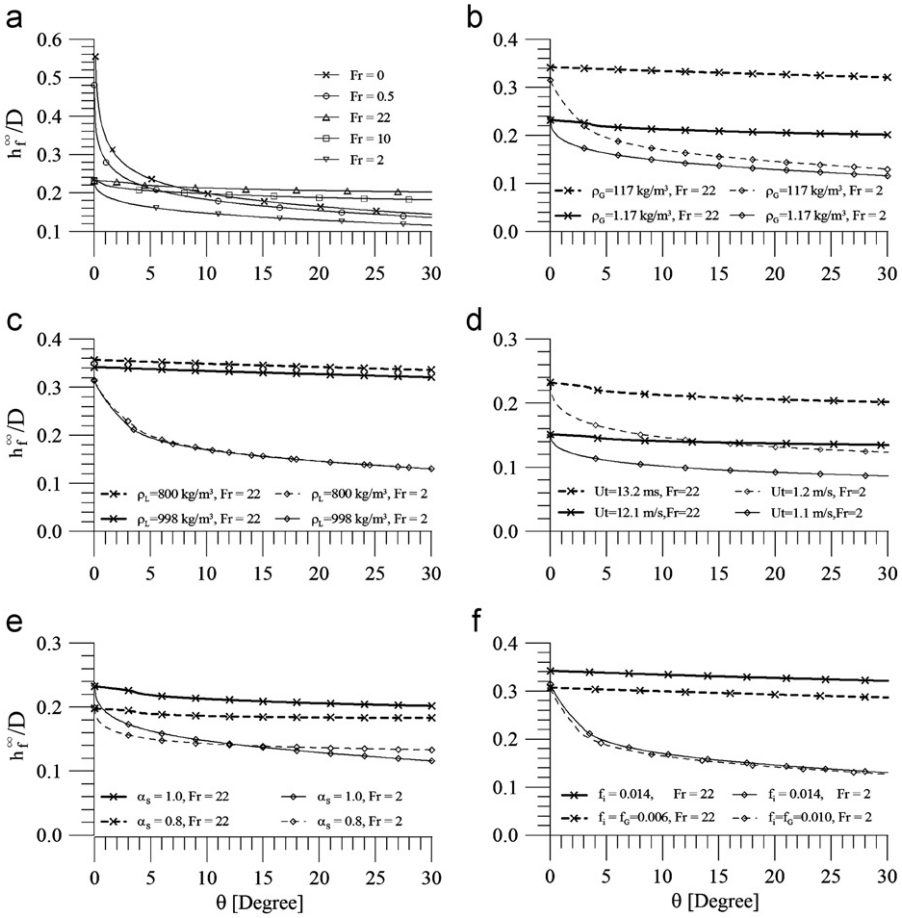

Fig. 5. Influence on the film equilibrium height for (a) Fr_M; (b) pressure; (c) ρ_L; (d) U_t; (e) α_S and (f) friction factor, at several pipeline inclinations.

It is known in advance that the equilibrium height is sensitive to the bubble translation velocity. The changes on U_t may arise from changes on the mixture velocity or also from changes on the C_0 and C_∞ parameters which in turn depend on the mixture Reynolds and Froude numbers, see Table 5. To avoid a cumbersome analysis involving u_M, C_0 and C_∞ it was chosen to change only U_t instead. Fig. 5d displays the equilibrium height as a function of the pipe inclination at distinct bubble translation velocity. The thin and the thick continuous lines represent Fr_M of 2 and 22 which exhibits a corresponding U_t of 1.1 and 12.1 m/s, all the other flow conditions follow the default conditions. On the other hand, the thin and thick dashed lines also represent Fr_M of 2 and 22 but have a corresponding U_t of 1.2 and 13.2 m/s. Once the Fr_M are kept constant, the differences among the velocities allude for differences on C_0 and C_∞ which may result from unlike closure relations. When U_t has increased to 9% Fig. 5d shows that the equilibrium height suffers an increase of 53% when the pipe at the horizontal regardless if Fr_M is of 2 or 22. As the pipe inclination changes to 30° the equilibrium height increases of 42% if Fr_M is of 2 and 50% if Fr_M is of 22.

The sensitivity of the equilibrium height on the liquid piston holdup for different pipe inclinations is shown in Fig. 5e. The holdup closure relations presented in Eqs. (45) and (46) depend on distinct flow parameters which lead to a mismatch on their estimates. Instead of using either one of them to estimate the model's sensitivity to holdup changes it was chosen to keep constant all parameters but reduce α_S from 1 to 0.8, here considered to be a lower bound to the averaged liquid piston holdup. This setup may lack physical realism but will render in a straightforward way the influence of α_S on the equilibrium height. The thin and thick continuous lines represent Fr_M of 2 and 22 for $\alpha_S=1$, a non-aerated liquid piston. Complementary, the thin and the thick dashed lines have the same definitions of the previous cases but are evaluated at $\alpha_S=0.8$. When the liquid piston holdup changes to 0.8 the growth rate of the equilibrium height with the pipe inclination decreases. Notice that the curves for $\alpha_S=1$ and $\alpha_S=0.8$ for Fr_M of 2 intercept each other at 13° approximately. At pipe inclinations lower than 13° the curve with 0.8 liquid holdup (thin dashed line) is always below the curve with holdup of 1. At pipe inclinations greater than 13° this behavior is reversed. At Fr_M of 22 the curves do not intercept each other; the curve for $\alpha_S=0.8$ has always a lower equilibrium height as compared to the $\alpha_S=1$ but with a smaller growth rate. The greatest differences among the curves happen for horizontal flows and are nearly 18%.

The interfacial friction factor is not a settled issue. As pointed in Section 2.8 the appearance of interfacial waves makes difficult the development of a theory for an accurate determination of the interfacial friction factor. Nowadays there are two propositions frequently employed to determine f_i which are: $f_i=0.014$ and $f_i=f_G$. The effects of f_i on the equilibrium height are felt only for high pressure operation otherwise the contribution of the gas and interfacial friction terms are negligible, likewise the sensitivity study developed to the liquid phase density. Fig. 5f shows the equilibrium height as a function of the pipe inclination for operation at 10^7 Pa and employing $f_i=0.014$ and $f_i=f_G$. The thin and the thick continuous lines are evaluated using $f_i=0.014$ and represent, respectively, the flow conditions at Fr_M of 2 and 22. The thin and the thick dashed lines mirror the previous flow parameters except that $f_i=f_G$. As observed in Fig. 5f the equilibrium heights evaluated using $f_i=0.014$ tend to the higher

than those evaluated using $f_i=f_G$. This effect is almost indistinguishable for Fr_M of 2 but the differences attain 13% when Fr_M is 22.

The main features of the sensitivity analysis are briefed accordingly to the applied operational conditions and closure equations. The sensitiveness of the equilibrium height to the pipe inclination is dependent on the Fr_M regime, see Fig. 5a. At low Froude, typically $Fr_M<2$, the equilibrium height is strongly sensitive to the pipe inclinations near off the horizontal. At high Froude, typically $Fr_M>10$ the equilibrium height is weakly dependent on the pipe inclination. At near atmospheric pressure the influence of the friction forces due to the gas phase and interface are negligible and the approximation embodied on the work of Dukler and Hubbard (1975) is valid. At high pressure, 10^7 Pa, the gas density comes to play on the force balance increasing the contribution of the gas and interface friction forces and diminishing the influence of the gravity term. The equilibrium height increases as the gas density increases or the liquid density decreases. The change on the equilibrium height gets bigger as the Fr_M increases, as shown Fig. 5b and c. The increase on the bubble translational velocity produces an increase on the equilibrium height, Fig. 5d. This behavior, already predicted for horizontal flow by Eq. (58), is now confirmed to all pipe inclinations analyzed. As the liquid slug holdup decreases from unity to 0.8 the equilibrium film thickness can be higher or lower than the film thickness observed when $\alpha_S=1$, see Fig. 5e. In fact the decrease of the liquid slug holdup decreases the growth rate of the equilibrium film height. Its behavior depends on the Froude regime. At last, the differences on interfacial friction factor on the equilibrium height, as displayed in Fig. 5f, are felt only on high pressure operation, likewise U_t and α_S, its effect increases as Fr_M increases.

5.3. Model sensitivity: analysis based on the liquid film profile

This section develops a limited analysis on the model's sensitivity based on the liquid film profile. Its aim is to explore the film shape sensitivity instead of a single point as represented by the equilibrium height. Only two parameters are chosen to this analysis: the bubble's nose velocity and the liquid phase viscosity. The first parameter was picked up because the analysis developed in Section 5.2 reveals that the bubble's nose velocity has a strong influence on the equilibrium height. The last parameter was selected for completeness since its analysis was not covered in Section 5.2. The analysis employs the film equation and the closure equations as stated at the beginning of Section 5 unless stated otherwise. It applies to a horizontal pipe, 26 mm ID, with an air–water mixture flowing at atmospheric pressure and ambient temperature.

The sensitivity of the liquid film profile to the bubble's nose velocity is developed for a mixture with air and water superficial velocities respectively of 1.67 and 0.33 m/s, and with non-aerated liquid slugs, i.e., $\alpha_S=1$. For reference, these flow conditions correspond to Re_M, Fr_M and Eo respectively of 52 000, 4 and 94. At these flow conditions the bubble's nose velocity has no drift since $Fr_M>3.5$ and its velocity depends only on the distribution parameter, C_0, which for turbulent regime is 1.2. The liquid film profiles are shown in Fig. 6a for a bubble with 100D. The continuous line apply to the default closure equations while the dashed line represents a case subjected to the same conditions but $C_0=1.12$. This value of C_0 was chosen because it was found experimentally for a 26 mm ID horizontal pipe with air and water mixture in our experimental facility and, being 6.6% less than 1.2, it becomes a good parameter to access the sensitivity. As C_0 changed from 1.2 to 1.12 the liquid film profile became thinner, as predicted by Eq. (58). The differences between the dimensionless height profiles range from 0.2 to 0.1 as the film coordinate, x_f/D, spans from 0 to 100. The greater differences are near the origin but they quickly decrease to nearly 0.1 when $x_f/D>40$. The differences on the film height profile result in an averaged film holdup of 0.33 and 0.22 when C_0 changes from 1.2 to 1.12, respectively. The difference of 50% might result in large mass imbalance and compromise the performance of general slug flow models.

the differences in the liquid phase viscosity may arise if the heat transfer is not properly accounted for. The liquid film model sensitivity to the liquid viscosity is shown in Fig. 6b. The film profiles are estimated for a liquid–gas mixture with superficial velocities of 0.33 and 1.67 m/s with three liquids: water and two oils with densities and viscosities of (800 kg/m^3 and 5.2×10^{-3} Pa s) and (800 kg/m^3 and 34.5×10^{-3} Pa s). The mixture Reynolds numbers are of 52 000, 8000 and 1200, respectively while the mixture Froude number is 4. Considering the cases with liquid slugs within the turbulent regime ($Re\geq8000$), one observes that the increase of the liquid viscosity by a factor of 5.2 displaces the dimensionless height profile upward almost uniformly along the film length by an amount of 0.05. The major differences are at the beginning of the film. As the film approaches equilibrium, $x_f/D>60$, the h_f differences diminish to values less than 0.02D. These differences on the film profile, although small, still causes variations on the averaged film holdup estimates of 10% which, by its turn, may introduce a large mass imbalance. As the liquid viscosity is further increased by a factor of 6.6 the liquid slugs are now in the laminar regime ($Re=1200$) and large differences on the film profiles are observed in Fig. 6b. In this scenario, the differences are not only due to the increase of the liquid viscosity, but mainly due to the change of turbulent to laminar flow regime which causes the distribution parameter to increase from 1.2 to 2. Summarizing, as long as the liquid slugs are in the turbulent regime, the increase of the liquid phase viscosity has small influence on the film profile. On the other hand, if the liquid viscosity increases to cause a change on the liquid slug regime then large differences are expected on the film profile due to the changes on the bubble velocity distribution parameter.

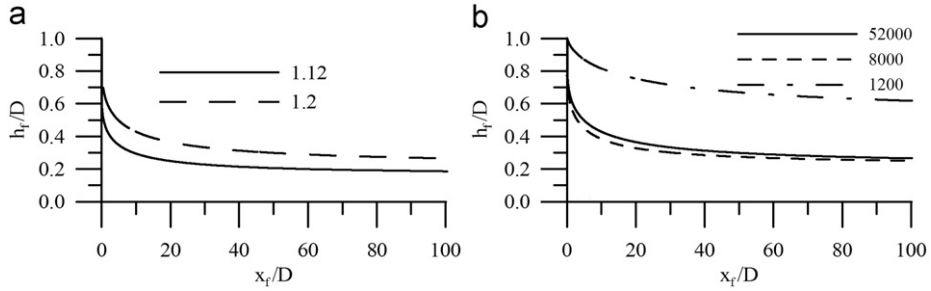

Fig. 6. Model sensitivity to (a) C_0; (b) mixture Reynolds.

5.4. Comparison against experimental data for horizontal flow

A limited test campaign limited to horizontal flow at Froude 4 was undertaken with the sole objective to check how the intermittent behavior of a continuous train of slugs affects the liquid film model performance. The alternating liquid pistons and gas bubbles which characterize the slug flow are not periodic in space neither in time. This section explores this non-deterministic flow feature testing if model still captures the liquid film profiles which have different lengths and bubbles' velocities.

One experimental run was taken at the horizontal test facility to get the film length, the film height profile and the bubble's nose velocity of each individual bubble that passed by the twin parallel wire probes placed at 777D downstream of the water–air mixer. The test conditions were at near atmospheric pressure and ambient temperature of 94.7 kPa and 23°C with mixture velocity of 1.92 m/s with the air to water ratio of 2:1 and Re, Fr, Eo of 52 000, 4, 95, see Table 7. Negligible air content was visually identified within the liquid slugs, therefore $\alpha_S=1$ was assumed. The averaged film height associated with the ith bubble, $\overline{h_f^i}$, is evaluated by post-processing the experimental data of the acquired film profile through:

$$\overline{h_f^i}=\frac{1}{L_f^i}\int_0^{L_f^i} h_f^i\,dx_f^i. \tag{59}$$

To better characterize the stochastic film properties: film length, averaged film height and bubble's nose velocity were determined for each single bubble. The total data amounts to 540 samples and have their variability shown in Fig. 7 as the pdf of the film length, film height and bubble's nose velocity. The velocity distributions are symmetrical, single peaked and centered close to the mixture velocity. The averaged U_t is 2.13 m/s. The film length distributions are skewed toward positive values of $\overline{L}_f/D$ with averaged value of 41. Finally the averaged film heights' distributions are symmetrical and single peaked with minimum and maximum dimensionless heights between 0.3 and 0.5 and averaged value of 0.35. For reference the distributions averaged values are presented in Table 7.

To explore the random nature of the experimental liquid film data the film model and the default closure equations are employed as defined at the beginning of Section 5. Two tests are devised to access the model's capability to capture: (i) the liquid film profile of an individual bubble out of a bubble population and (ii) the averaged liquid film height of each single bubble found on the bubble population. In short they are identified as Experimental Test no. 1 and no. 2.

Table 7
Averaged parameters for the experimental run.

Run	u_M	J_L	J_G	$\overline{L}_f/D$	$\overline{h}_f/D$	$\overline{U}_t$	Re	Fr	Eo
#2	1.92	0.67	1.25	41	0.35	2.13	52000	4	95

The Experimental Test no. 1 uses a film height profiles picked at random from the experimental run, see scatter plot on Fig. 8. The film height model employs three values for U_t corresponding to the fitted velocity (see Table 5), the averaged bubble's nose velocity arising from the sample (see Table 7) and the measured bubble's nose velocity of the specific chosen film. For reference these values are 2.30, 2.13 and 2.17 m/s. Notice that none of the three velocities' values are coincident. In fact they should not necessarily be because the first and the second values of U_t represent, respectively, the fitted and the averaged values while the third comes from a normal like distribution, see Fig. 7. The film profile estimates based on the sequence of U_t values, first to third, are represented in Fig. 8 by dash-point-dash, dashed and continuous line, respectively. As observed in Fig. 8, the best film estimate arises when it is employed the bubble's nose velocity belonging to the particular chosen bubble followed by the estimate when its averaged value is used. At the nose region of the bubble the model is expected to fail as seen in the figure when $x_f/D<5$ but it fits well the bubble's body region, $x_f/D>5$. Surprisingly, the result shows that the liquid film model still captures the film profile of a individual bubble in continuous slug flow despite the existing bubble-to-bubble interactions which may introduce free oscillations due to gas compressibility, bubble coalescence and the flow disturbances caused by the continuous slug formation at the water–air injector and slug disappearance at the pipe's discharge. It must be observed though, that the success of the model is due to the knowledge of the specific bubble's nose velocity. This experimental evidence reassures the results of the sensitivity analysis which demands accurate estimates of U_t to get good estimates for the film profile. It is acknowledged that the

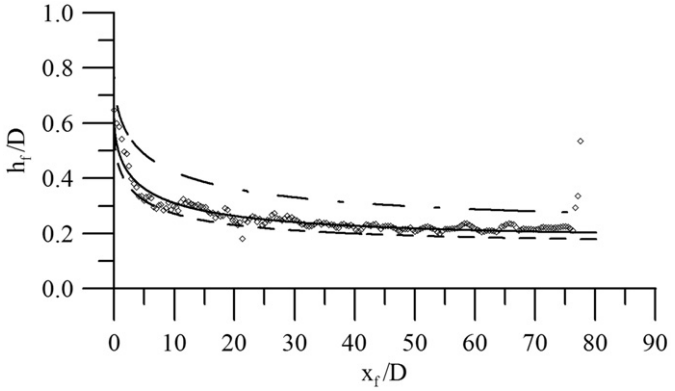

Fig. 8. Film height versus the film length of a single bubble. Legend: ◇ experimental data, ———— experimental bubble velocity, — — — — · experimental averaged bubble velocity and — · · — · · — fitted bubble velocity (Table 5).

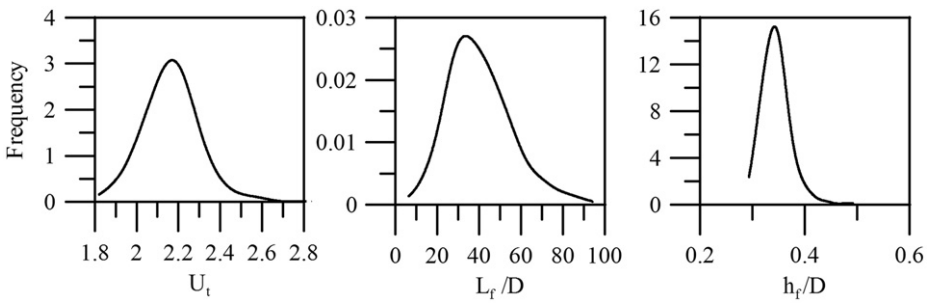

Fig. 7. Probability density functions for U_t, L_f/D and h_f/D for $J_L=0.67$ m/s and $J_G=1.25$ m/s.

value of U_t for each particular bubble is not always available off hand but, if one has it by experimental measurement, for example, the film model can capture the particular bubble profile.

The lack of success to predict the film profile at the bubble's nose region is not only the fault of the film model but it is also due to the lack of reliability of the experimental technique under certain condition. If one assumes that the liquid phase always occupies the lower section of the pipe, then the parallel wire probe measures it correctly. But, if the bubble's nose moves toward the center of the pipe, as in fact it does when the mixture velocity increases, then the measured nose profile is incorrect because the liquid occupies the lower and the upper sections of the pipe. A photograph of the bubble's nose at the test conditions is in Fig. 9 showing a nose profile displaced toward the pipe centerline with liquid above and below the gas–liquid interface. This experimental evidence sheds suspicion on the reliability of the film height measurements near at the bubble's nose.

The Experimental Test no. 2 employs the population of 540 film profiles to get the averaged film height and film length of each sampled bubble. The experimental data are shown in Fig. 10 as a scatter plot with the averaged film height of each sampled bubble on the y axis while the x axis displays its corresponding film length. As expected the averaged film height decreases as the film length increases. The Experimental Test no. 2 was devised to access the film model's capability to capture the tendency of the averaged film height population with the corresponding film length.

This task requires the information about the averaged liquid height and the length of the liquid film population. This information can be retrieved immediately considering that bubbles with different volumes, but with the same mixture velocity, lay on the same basic profile, Fagundes Netto et al. (1999). Resorting to this geometrical property then it is possible to run once the film model and get the averaged film height as the marching procedure advances over the film length. The numerical simulation employs the film equation and the closure equations as stated at the beginning of Section 5. To improve the quality of the estimate the experimental averaged bubble's nose velocity is used, as given in Table 7, instead of getting U_t from the default closure equations. The averaged film height, $\overline{h_f}$, corresponding to a film length L_f is determined by integrating the film profile up to L_f accordingly to an expression similar to Eq. (59):

$$\overline{h_f}(L_f) = \frac{1}{L_f}\int_0^{L_f} h_f(x_f)\,dx_f. \tag{60}$$

The definition of Eq. (60) implies that the film model captures the film height from the nose to the tail of the bubble. Acknowledging that the model applies to the bubble's body only, the averaged process has to be split into two parts: one regarding to the bubble's nose region and the other to the bubble's body. The bubble's tail is neglected. Under these assumptions the averaged film height as a function of the film length turns to be

$$\overline{h_f}(L_f) = \frac{(L_f - x_N)\left\{\frac{1}{(L_f - x_N)}\int_{x_N}^{L_f} h_f(x_f)dx_f\right\} + x_N\overline{h_{f,N}}}{L_f}, \tag{61}$$

where x_N and $\overline{h_{f,N}}$ represent the bubble's nose length and averaged its height respectively.

To get $\overline{h_f}(L_f)$ from Eq. (61) it is necessary to know x_N and $\overline{h_{f,N}}$ in advance or consider that the bubble's nose contribution to the averaged process is negligible, i.e. $x_N/L_f \ll 1$. For long films' approximations, $x_N/L_f \ll 1$, Eq. (61) reduces to Eq. (60) which is ready to be integrated employing the film model. The long film approximation is represented in Fig. 10 by the dashed line. It fits the film heights for long films, $L_f/D > 60D$, but fails for short films where the weight of the bubble's nose length is no longer negligible on the average process.

With the resource of the experimental data it is possible to estimate Eq. (61). The contribution of the film length and height belonging to the bubble's nose region is taken as the experimental data $(x_N, \overline{h_{f,N}})$ coming from the shortest film which are (7D, 0.40), respectively. This procedure was implemented to the evaluation of the dimensionless average film height and the result is shown in Fig. 10 as a continuous line. As observed in Fig. 10, there is an improvement on the averaged film height estimates, especially for short films. For long films the two curves approach each other asymptotically.

The experimental data, although limited to horizontal flows, has proved the film model capability to capture the averaged film heights of individual bubbles coming from a non-uniform population. If the information regarding the bubble's nose properties is available then Eq. (61) can be solved in full and the estimates have a good match against the experimental data. Otherwise one has to use the long film approximations which still compares well against the experimental data as long as $L_f/D > 60$.

Fig. 9. Photograph of the bubble's nose for $J_L = 0.67$ m/s and $J_G = 1.25$ m/s.

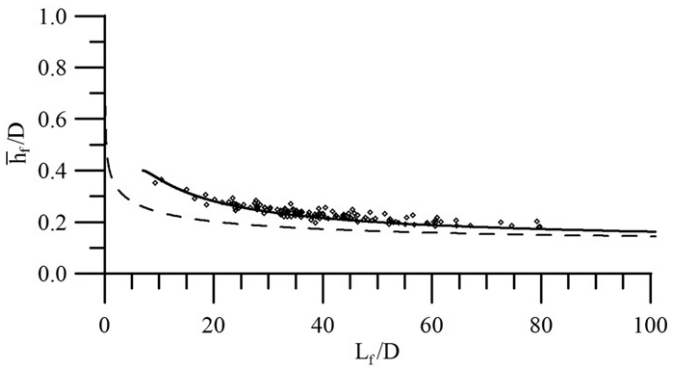

Fig. 10. Averaged film height versus the film length. Legend: ◇ experimental data, ———— model estimate supplying bubble's nose information, — — — — · model estimate employing long film approximation.

6. Conclusions

Despite of the liquid film models being represented by expressions which are quite distinct from each other they all share the same momentum equations which are casted in a single equation either in terms of the liquid film holdup or of the film height. In regard to the physical terms represented on the formulations the DH and NAG are the simplest models acknowledging only the liquid phase contribution to the momentum equation. The KS model adds to DH and NAG models the contribution of the interfacial shear term. The ABN model is the only model which applies to aerated and non-aerated liquid films, all the other models apply to non-aerated liquid films. This model keeps all terms already listed by the previous models and partially includes the contribution of the gas phase terms, i.e., keeps the shear stress but neglects the inertia and hydrostatic. The CB model adds to the ABN the gas phase inertia but still neglects the gas phase hydrostatic term. The FFP model applies to horizontal flows only and only neglects the gas phase inertia terms. Finally, the TB model acknowledges the contribution of all physical terms

of the separated phase momentum equation. In terms of formulations all models, with the exception of TB, can be considered as approximations of the full momentum equations which partially or completely neglect the terms related with the gas phase and interfacial shear stress.

The comparative test among all models showed that for low pressure and moderate Froude numbers these approximations embodied on the formulations give out equally good results as the full term formulation. This can benefit some liquid film model application which, by using a simpler formulation like the one proposed by Dukler and Hubbard (1975), still gets good estimates. Differences among the formulations arise when the pressure increases. In this scenario the interfacial shear stress term is no-longer negligible. The major source of disagreement on the models lies on the closure relations. It was seen that the liquid film models are quite sensitive to changes in the bubble's velocity and also on the liquid slug holdup. Inaccuracies on these parameters lead to differences on the estimates of α_f or h_f.

The sensitivity analysis based on the equilibrium height of film disclosed that the model is sensitive to the pipe inclination for low Froude numbers. As the Froude number increases the film height becomes almost constant as the pipe inclination changes from horizontal up to 30°. The effects of the gas density and interfacial friction factor are felt on the film height only for high pressure operation. The analysis also detected that the film height is most sensitive to the bubble's nose velocity.

The experimental data although limited to horizontal flow at Froude of 2 and 4, showed that the liquid film model captures the instantaneous liquid film profile out of a continuous train of slugs as well as the trend between the average film height and its corresponding length. The success of the test reaffirms that the film model embodies the correct physics of the phenomena but it demands accurate estimate of the bubble's nose velocity, liquid slug hold up and interfacial friction factor often not matched by general fit equations.

Acknowledgments

The authors gratefully acknowledge the research grant from Petrobras, under contract no. 00500029781.07.2; also Yoshizawa, C.J. thanks the received scholarship from CAPES during 2004–2006.

References

Abdul-Majeed, G.H., 2000. Liquid slug holdup in horizontal and slightly inclined two-phase slug flow. J. Pet. Sci. Eng. 27, 27–32.

Alves, I.N., Shoham, O., Taitel, Y., 1993. Drift velocity of elongated bubbles in inclined pipes. Chem. Eng. Sci. 48 (7), 3063–3070.

Al-Safran, E.M., Taitel, Y., Brill, J.P., 2004. Prediction of slug length distribution along a hilly terrain pipeline using slug tracking model. Journal of Energy Resources Technology 126 (1), 54–62.

Abiev, R.Sh., 2008. Simulation of the slug flow of a gas–liquid system in capillaries. Theor. Found. Chem. Eng. 42 (2), 105–117.

Andreussi, P., Bendiksen, K.H., Nydal, O.J., 1993. Void distribution in slug flow. Int. J. Multiphase Flow 19, 817–828.

Barnea, D., Brauner, N., 1985. Holdup of the liquid slug in two phase intermittent flow. Int. J. Multiphase Flow 11, 43–49.

Barnea, D., Taitel, Y., 1993. A model for slug length distribution in gas–liquid slug flow. Int. J. Multiphase Flow 19 (5), 829–838.

Bendiksen, K.H., 1984. An experimental investigation of the motion of long bubbles in inclined tubes. Int. J. Multiphase Flow 10 (4), 467–483.

Benjamin, T.B., 1968. Gravity currents and related phenomena. J. Fluid Mech. 31, 209–248.

Bretherton, J.P., 1961. The motion of long bubbles in tubes. J. Fluid Mech. 10, 166–188.

Cohen, L.S., Hanratty, T.J., 1968. Effect of waves at a gas–liquid interface on a turbulent air flow. J. Fluid Mech. 31, 467–479.

Cook, M., Behnia, M., 2001. Bubble motion during inclined intermittent flow. Int. J. Heat Fluid Flow 22, 543–551.

Cook, M., Behnia, M., 1997. Film profiles behind liquid slugs in gas–liquid pipe flow. A.I.Ch.E. J. 43 (9), 2180–2186.

De Henau, V., Raithby, G.D., 1995a. A transient two-fluid model for the simulation of slug flow in pipelines—I. Theory. Int. J. Multiphase Flow 21 (3), 335–349.

De Henau, V., Raithby, G.D., 1995b. A transient two-fluid model for the simulation of slug flow in pipelines—II. Validation. Int. J. Multiphase Flow 21 (3), 351–363.

Dukler, A.E., Hubbard, M.G., 1975. A model for gas–liquid slug flow in horizontal and near horizontal tubes. Ind. Eng. Chem. Fundam. 14 (14), 337–347.

Ellis, S.R.M., Gay, B., 1959. The parallel flow of two fluid streams: interfacial shear and fluid–fluid interaction. Trans. Instn. Chem. Eng. 37, 206–213.

Fagundes Netto, J.R., Fabre, J., Paresson, L., 1999. Shape of long bubbles in horizontal slug flow. Int. J. Multiphase Flow 25, 1129–1160.

Fernandes, R.C., Semiat, R., Dukler, A.E., 1983. Hydrodynamic model for gas–liquid slug in vertical tubes. A.I.Ch.E. J. 29 (6), 981–989.

Gregory, G.A., Nicholson, M.K., Aziz, K., 1978. Correlation of the liquid volume fraction in the slug for horizontal gas–liquid slug flow. Int. J. Multiphase Flow 4, 33–39.

Grenier, P., 1997. Evolution des longueurs de bouchons en écoulement intermittent horizontal. Ph.D. Thesis, Institut national polytechnique de Toulouse (INPT).

Gomez, L.E., Shoham, O., Taitel, Y., 2000. Prediction of slug liquid holdup: horizontal to upward vertical flow. Int. J. Multiphase Flow 26, 517–521.

Ishii, M., Hibiki, T., 2006. Thermo-Fluid Dynamics of Two-Phase Flow. Springer, NY.

Kokal, S.L., Stanislav, J.F., 1989. An experimental study of two-phase flow in slightly inclined pipes—II: liquid holdup and pressure drop. Chem. Eng. Sci. 44 (3), 681–693.

Koskie, J.E., Mudawar, I., Tiederman, W.G., 1989. Parallel-wire probes for the measurement of thick liquid films. Int. J. Multiphase Flow 15 (4), 521–529.

Kreutzer, M.T., Kapteijn, F., Moulijn, J.A., Kleijn, C.R., Heiszwolf, J.J., 2005. Inertial and interfacial effects on pressure drop of Taylor flow in capillaries. A.I.Ch.E. J. 51, 2428–2440.

Nicholson, M.K., Aziz, K., Gregory, G.A., 1978. Intermittent two phase flow in horizontal pipes: predictive models. Can. J. Chem. Eng. 56, 653–663.

Nydal, O.J., Banerjee, S., 1994. Dynamic slug tracking simulations for gas–liquid flow in pipelines. Chem. Eng. Commun. 141 (1), 13–39.

Oliemans, R.V.A., Pots, B.F.M., 2006. Gas liquid transport in ducts. In: Crowe, C.T. (Ed.), Multiphase Flow Handbook. CRC Press, Boca Raton.

Pauchon, C.L., Dhulesia, H., Binh-Cirlot, G., Fabre, J., 1994. TACITE: a transient tool for multiphase pipeline and well simulation, SPE Annual Technical Conference and Exhibition (SPE 28545), New Orleans, USA.

Ruder, Z., Hanratty, T.J., 1990. A definition of gas–liquid plug flow in horizontal pipes. Int. J. Multiphase Flow 16, 233–242.

Straume, T., Nordsven, M., Bendiksen, K., 1992. Numerical simulation of slugging in pipelines. Multiphase Flow in Wells and Pipelines, ASME 144, 103–112.

Taitel, Y., Barnea, D., 1990. Two-phase slug flow. Adv. Heat Transfer 20, 43–132.

Viana, F., Pardo, R., Yánez, R., Trallero, J.L., Joseph, D.D., 2003. Universal correlation for the rise velocity of long gas bubbles in round pipes. J. Fluid Mech. 494, 379–398.

Wallis, G.B., 1969. One-Dimensional Two-Phase Flow. McGraw-Hill Book Comp., New York.

Weber, M.E., 1981. Drift in intermittent two-phase flow in horizontal pipes. Can. J. Chem. Eng. 59, 398–399.

Zhang, H.-Q., Wang, Q., Sarica, C., Brill, J.P., 2003. An unified mechanistic model for slug liquid holdup and transition between slug and dispersed bubble flows. Int. J. Multiphase Flow 29, 97–107.

Zuber, N., Findlay, J.A., 1965. Average volumetric concentration in two-phase flow systems. J. Heat Transfer 87, 453–468.